

Pro gradu -tutkielma

Teoreettinen fysiikka

Four-loop Feynman diagrams in three dimensions

Aleksi Vuorinen

2001

Ohjaaja: Prof. Keijo Kajantie

Tarkastajat: Prof. Keijo Kajantie, Prof. Claus Montonen

HELSINGIN YLIOPISTO
FYSIKAALISTEN TIETEIDEN LAITOS

PL 64
00014 Helsingin yliopisto

Acknowledgements

I would like to thank Keijo Kajantie for being my supervisor and for giving me invaluable advice not only during the writing of this thesis but in the whole course of my university studies. In addition I wish to express my gratitude to York Schröder, who has helped me a great deal in the diagrammatic calculations and on whose work much of the material of chapters 4-6 is based. During the past year my student friends Antti Gynther, Tuomas Lappi and Mikko Vepsäläinen have taught me a lot of physics and showed what being a physicist is all about. They certainly must be acknowledged. There are also other students, such as Janne Högdahl, Jonna Koponen, Vesa Muhonen and Teemu Ojanen, with whom I have often discussed matters at least remotely related to physics and who I want to thank. A special thanks naturally belongs to my parents for all their support.

Contents

| | | |
|----------|--|-----------|
| 1 | Introduction | 1 |
| 2 | The free energy of hot QCD | 4 |
| 2.1 | QCD at finite temperatures | 4 |
| 2.2 | Dimensional reduction and effective QCD | 7 |
| 2.3 | The three-dimensional free energy | 12 |
| 2.4 | The skeleton expansion | 17 |
| 3 | Evaluation of scalar diagrams in three dimensions | 20 |
| 4 | Diagrams evaluated in momentum space | 22 |
| 4.1 | Diagram <i>a</i> | 22 |
| 4.2 | Diagram <i>b</i> | 24 |
| 4.3 | Diagram <i>c</i> | 24 |
| 5 | Diagrams evaluated in coordinate space | 25 |
| 5.1 | Preliminaries | 25 |
| 5.2 | Diagram <i>d</i> | 26 |
| 5.3 | Diagram <i>e</i> | 28 |
| 6 | The remaining diagrams | 37 |
| 6.1 | Numerical calculations | 37 |
| 6.2 | Partial differential equations | 41 |
| 7 | Conclusions | 43 |

Chapter 1

Introduction

Richard P. Feynman is quoted saying "the purpose of physics is to produce numbers". One of the most interesting numbers concerning QCD, the theory of strong interactions, is the value of its free energy as a function of temperature. The purpose of this master's thesis is to explore the process of improving the perturbative expansion of this quantity. By providing results for previously unevaluated four-loop scalar Feynman diagrams I also hope to be able to make a small contribution to this work.

Soon after the rapid development of the theoretical structure of QCD in early 1970's [1] it was proposed that when a hadronic system is heated or compressed enough, one will at some point observe a dramatic change in its physical properties [2]. This would happen when the wave functions of the hadrons start overlapping and would lead to a transition of the system from a low-temperature phase of baryons and mesons to a high-temperature phase described by a gas of free quarks and gluons. The setup has since then been studied intensively and there now exists strong evidence suggesting that at a critical temperature of $T_c \approx 170$ MeV QCD matter indeed undergoes a deconfining phase transition into quark-gluon plasma [3]. The reason for the importance of having an accurate theoretical prediction for the free energy at $T > T_c$ is that it affects the probes used in studying the phase transition e.g. in heavy-ion collisions. This is a very hot topic in the current research of high energy physics, since summer 2000 witnessed the start of a new and powerful heavy-ion collider RHIC at Brookhaven, New York. Another collider designed for colliding massive hadronic particles, LHC, is currently being built at CERN and will hopefully start producing data in 2006.

The theoretical study of finite temperature QCD matter has traditionally employed two very distinctive methods: high T perturbation theory [4, 5] and lattice simulations [6, 7]. The latter approach is non-perturbative but is very difficult to apply if dynamical quarks are present or, especially, if the baryon chemical potential is nonzero [8]. It has however been successfully used in evaluating the $\mu_B = 0$, $N_f = 0$ free energy at a temperature scale ranging from below the critical temperature up to a few times T_c [9, 10]. Perturbative QCD is, on the other hand, a method based on expanding different physical quantities with respect to the gauge coupling g , and is most easily applied in the region $T \gg T_c$, where g is small. This is a serious limitation since one is in general not only interested in the limit of asymptotically high temperatures, where the plasma behaves almost like an ideal gas, but

also in temperatures near T_c . Another setback comes from the fact that e.g. the free energy gets contributions from different momentum scales ranging from T down to g^2T so that the problem is a multiscale one: even if g were small at energies of order T its value may well be considerably larger at other relevant scales.

In order to be able to extend the perturbative regime of the free energy down to the interesting region of temperatures of only a few times T_c , one is forced to tackle the technically very demanding calculation of high-order terms in the corresponding perturbation expansion. A straightforward evaluation of these terms in full thermal QCD is, however, not sufficient all the way, since the loop expansion of F breaks down at order g^6 [11]. An efficient approach for solving the problem is offered by the construction of effective three-dimensional field theories [12, 13], which can be used to extract the contributions of small momenta. These theories can in turn be studied by a combination of analytic calculations and lattice simulations [14].

At high perturbative orders it becomes necessary to evaluate large numbers of multi-loop Feynman diagrams in the effective theory. Reaching beyond order g^5 in the free energy expansion one is faced among other things with the challenge of calculating numerous four-loop vacuum diagrams in a three-dimensional 'SU(3) + adjoint Higgs' theory without fermions [15]. A software capable of simplifying complicated tensor products, such as FORM [16], can be used to reduce these into a set of four-loop scalar diagrams containing powers and scalar products of loop momenta in the numerators of the corresponding integrands. The evaluation of a subset of these is the main goal of my thesis.

The calculation of multi-loop scalar diagrams constitutes an interesting area of research as such and has been approached by many authors both in three and four dimensions: [13, 17, 18, 19, 20] to name a few. The diagrams have applications in various field theories their use ranging from finite temperature QCD to condensed matter physics. They become necessary whenever a perturbative expansion is performed with respect to a parameter of finite magnitude and numerically accurate predictions are sought after. In this thesis my objective is to evaluate all non-trivial four-loop 2PI (two-particle irreducible) vacuum diagrams of a scalar theory containing couplings of any number of particles. There are altogether ten such diagrams of different topology and I shall calculate them analytically and with arbitrary masses of propagators whenever possible. As a regularization scheme for ultraviolet divergencies I am going to use dimensional regularization, i.e. work in $3 - 2\epsilon$ dimensions, which will in the case of divergent diagrams result in Laurent expansions with respect to ϵ .

The thesis is organized as follows. Chapter 2 presents an overview of the properties of the QCD free energy and explores its evaluation in more detail. After briefly reviewing the formalism used in finite temperature quantum chromodynamics I concentrate in section 2.1 on the history and present status of the research aimed at finding F . In 2.2 I then explain the construction of the three-dimensional effective theories through dimensional reduction following to some extent the treatment of [21]. After that I concentrate on the recent work of Kajantie et al. [14, 22] and introduce in section 2.3 their setup for obtaining the three-dimensional free energy. In 2.4 I further review the skeleton method used in constructing loop expansions for this quantity and then conclude by explaining how the scalar diagrams evaluated in this thesis enter the calculations.

Chapters 3 to 6 are entirely devoted to the evaluation of the diagrams mentioned above. In chapter 3 I give a general introduction to the diagrammatic calculations and explain

the different notations and conventions. The integrals are then divided into three chapters based on the calculational method used: chapter 4 contains three diagrams evaluated directly in momentum space, chapter 5 two diagrams, results for which are obtained after Fourier-transformation into coordinate space and chapter 6 finally five diagrams with whom other methods have to be applied. In chapters 4 and 5 arbitrary masses are used on each propagator line and results are obtained either in the form of an analytic expression or as 1- or 2-dimensional integrals. For the diagrams of chapter 6 integral representations of various dimensions are constructed in the case where the masses are identical, and they are then evaluated numerically. In addition to this, first order partial differential equations with respect to the different masses are obtained for these diagrams with the exception of one graph. The topologies of the diagrams evaluated in this thesis are printed below.

$$\begin{aligned}
 \text{Diagrams of chapter 4 :} & \quad \text{[triangle in circle]}, \text{ [square in circle]}, \text{ [rectangle in circle]} . \\
 \text{Diagrams of chapter 5 :} & \quad \text{[two overlapping circles]}, \text{ [circle with internal lines]} . \\
 \text{Diagrams of chapter 6 :} & \quad \text{[circle with internal lines]}, \text{ [circle with cross]}, \text{ [two overlapping circles]}, \\
 & \quad \text{[rectangle in circle]}, \text{ [circle with internal lines]} . \tag{1.1}
 \end{aligned}$$

To conclude this introductory section I now mention a few general conventions that will be applied in the following. In all considerations of chapter 2 the masses of the relevant quarks as well as the net baryon density and the baryon chemical potential are assumed to be zero. The first condition is a valid approximation based on the small masses of the up and down quarks in comparison with T_c . The second constraint is, on the other hand, more severe since e.g. in heavy-ion collisions the net baryon density certainly does not vanish. The generalization of the perturbative calculations to the $\mu_B \neq 0$ -region is, however, in principle straightforward [23] and is not expected to alter the qualitative results significantly at least for small values of the chemical potential. As is customary in the literature I will hereafter make a choice of units such that $\hbar = c = k_B = 1$. This is merely a matter of convenience and can at any point be undone.

Chapter 2

The free energy of hot QCD

2.1 QCD at finite temperatures

Quantum chromodynamics is the gauge field theory that describes strong interactions. Its symmetry group is $SU(3)$ and it comprises of N_f families of quarks ψ_f^i in the fundamental representation and the gluons A_μ^i in the adjoint one. Here i and a stand for the color degrees of freedom and run from 1 to 3 for the spin-1/2 quarks and from 1 to 8 for the spin-1 gauge boson, gluon. N_f is not fixed but denotes the number of quark flavors relevant in each case. In Minkowskian metric the Lagrangian of QCD is

$$\mathcal{L}_{QCD} = -\frac{1}{4} F_{\mu\nu}^a F^{a\mu\nu} + \sum_f \bar{\psi}_f [i\gamma^\mu D_\mu - m_f] \psi_f, \quad (2.1)$$

where the quarks are represented by 4-component spinors in coordinate space and by 3-vectors in color space, and

$$\begin{aligned} F_{\mu\nu}^a &= \partial_\mu A_\nu^a - \partial_\nu A_\mu^a - gf^{abc} A_\mu^b A_\nu^c, \\ D_\mu &= \partial_\mu + igA_\mu^a T^a. \end{aligned} \quad (2.2)$$

Here the 3×3 matrices $T^a, a \in \{1, \dots, 8\}$ are the generators of $SU(3)$ (proportional to the Gell-Mann matrices).

The above Lagrangian is invariant under local $SU(3)$ gauge transformations. In their infinitesimal form the transformations read

$$\begin{aligned} A_\mu^a &\rightarrow A_\mu^a + gf^{abc} A_\mu^b \theta^c - \partial_\mu \theta^a, \\ \psi &\rightarrow (1 + ig\theta^a T^a) \psi, \end{aligned} \quad (2.3)$$

where $\theta^a, a \in \{1, \dots, 8\}$ are arbitrary infinitesimal functions of space-time. This invariance leads to problems when constructing a covariant zero-temperature perturbation theory for QCD, since one then needs some method of fixing the gauge in the functional integral corresponding to the generating functional of Green's functions. The gauge fixing is required in order to avoid an overcounting of physical degrees of freedom and is achieved by introducing unphysical anticommuting scalar particles, Faddeev-Popov ghosts $C^a, a \in \{1, \dots, 8\}$, in the

theory. In finite temperature QCD with zero baryon chemical potential one is eventually lead to a representation for the partition function in the form

$$Z \equiv \text{Tr} e^{-\beta H} = \int \mathcal{D}A_\mu^a \mathcal{D}\bar{\psi} \mathcal{D}\psi \mathcal{D}\bar{C}^a \mathcal{D}C^a \exp \left[\int_0^\beta d\tau \int d^3x \mathcal{L}_{eff} \right], \quad (2.4)$$

where

$$\mathcal{L}_{eff} = \mathcal{L}_{QCD} + \partial_\mu \bar{C}^a \partial^\mu C^a + g f^{abc} \bar{C}^a \partial_\mu A^{b\mu} C^c - \frac{1}{2\xi} (\partial_\mu A^{a\mu})^2. \quad (2.5)$$

Here $\beta \equiv 1/T$, time has here been rotated into an imaginary one $\tau = it$ and $-\frac{1}{2\xi} (\partial_\mu A^{a\mu})^2$ is the usual covariant gauge fixing term. As always in path integral representations of the partition function, the only bosonic fields that contribute are the ones periodic on the interval $0 \leq \tau \leq \beta$ and correspondingly the only contributing fermionic fields are the antiperiodic ones.

The functional integral in (2.4) cannot be evaluated analytically. It can, however, be used in calculating the different thermodynamic observables of QCD to different orders in finite temperature perturbation theory, where the coupling constant g is treated as a small expansion parameter ($g \ll 1$). This seems to be justified at high temperatures, since the lowest order solution to the renormalization group equation for g shows that the coupling decreases logarithmically as the energy scale μ is increased:

$$\alpha(\mu) \equiv \frac{g^2(\mu)}{4\pi} = \frac{6\pi}{(33 - 2N_f) \ln(\mu/\Lambda_{QCD})}. \quad (2.6)$$

Here Λ_{QCD} is an integration constant originating from the RGE and signaling the divergence of (2.6) at low momenta. Despite the above result, one must be careful in applying perturbation theory even at high T since different physical quantities receive contributions also from momentum scales considerably lower than T . Even if g were small at scale T thus allowing a perturbative treatment, the situation may well be different at the other relevant scales.

The simplest and at the same time the most fundamental observable of a high temperature system is its free energy density $f = \frac{F}{V} = -\frac{T}{V} \ln Z$, which determines various static thermodynamic quantities through standard equations of statistical mechanics. Since in the case of QCD f essentially equals the functional integral of (2.4), the whole finite temperature theory can be seen to be defined by its value as a function of T and the other parameters, such as coupling constants. Assuming the temperature to be high enough so that the masses of relevant quarks can be neglected one may write the perturbative expansion of f in the form [21] (μ being the renormalization scale)

$$f = -\frac{8\pi^2}{45} T^4 \left[F_0 + F_2 \frac{\alpha(\mu)}{\pi} + F_3 \left(\frac{\alpha(\mu)}{\pi} \right)^{3/2} + F_4 \left(\frac{\alpha(\mu)}{\pi} \right)^2 \ln \frac{\alpha(\mu)}{\pi} + F_5 \left(\frac{\alpha(\mu)}{\pi} \right)^2 + F_6 \left(\frac{\alpha(\mu)}{\pi} \right)^{5/2} + \mathcal{O} \left(\alpha^3(\mu) \ln \alpha(\mu), \alpha^3(\mu) \right) \right], \quad (2.7)$$

where the coefficients are

$$\begin{aligned}
F_0 &= 1 + \frac{21}{32} N_f \\
F_2 &= -\frac{15}{4} \left(1 + \frac{5}{12} N_f \right) \\
F_3 &= 30 \left(1 + \frac{1}{6} N_f \right)^{3/2} \\
F_4 &= \frac{135}{2} \left(1 + \frac{1}{6} N_f \right) \\
F_5 &= 237.2 + 15.97 N_f - 0.413 N_f^2 + \frac{135}{2} \left(1 + \frac{1}{6} N_f \right) \ln \left(1 + \frac{1}{6} N_f \right) \\
&\quad - \frac{5}{8} \left(1 + \frac{5}{12} N_f \right) (33 - 2N_f) \ln \frac{\mu}{2\pi T} \\
F_6 &= \left(1 + \frac{1}{6} N_f \right)^{1/2} \left(-799.2 - 21.96 N_f - 1.926 N_f^2 \right. \\
&\quad \left. + \frac{15}{2} \left(1 + \frac{1}{6} N_f \right) (33 - 2N_f) \ln \frac{\mu}{2\pi T} \right).
\end{aligned}$$

As can be easily verified using (2.6), the μ -dependence of (2.7) cancels between the different terms exactly in such a way that $\frac{d}{d(\ln \mu)} F = 0$ to the order shown. This is of course essential, since μ is not a physical parameter. The absence of an $\alpha(\mu)^{5/2} \ln \alpha(\mu)$ term from (2.7) is not immediately obvious but is due to remarkable cancellations that occur between various diagrams [24].

To zeroth order in the coupling a strongly interacting system consists of merely non-interacting quarks and gluons. Therefore the leading order term in the above expansion, F_0 , corresponds to the well-known result of the free energy of an ideal gas of 8 massless gauge bosons and $3N_f$ massless fermions (see e.g. chapter 17 of [25]). It depends on the number of colors but is otherwise independent of the structure of QCD. The first non-trivial coefficient, F_2 , is on the other hand already clearly characteristic to QCD and was evaluated by Shuryak in 1978 [26]. This required the calculation of a set of four 2-loop diagrams in thermal QCD:

$$F_2 \sim -\frac{1}{2} \text{[diagram 1]} - \frac{1}{2} \text{[diagram 2]} + \frac{1}{12} \text{[diagram 3]} + \frac{1}{8} \text{[diagram 4]}. \quad (2.8)$$

The coefficients F_3 and F_4 of the first non-analytic terms in the expansion were obtained, respectively, in 1979 by Kapusta [27] and in 1983 by Toimela [28]. The authors evaluated to leading order the Debye length for color charge, which describes the screening of the chromoelectric force. This involved calculating an infinite set of ring diagrams of the form:

$$\frac{1}{2} \left[\frac{1}{2} \text{[diagram 1]} - \frac{1}{3} \text{[diagram 2]} + \dots \right], \quad (2.9)$$

where the one-loop gluon self-energy reads

$$\text{[diagram 1]} = -\frac{1}{2} \text{[diagram 2]} - \frac{1}{2} \text{[diagram 3]} + \text{[diagram 4]} + \text{[diagram 5]}. \quad (2.10)$$

In addition there were three 3-loop diagrams that had to be obtained to get all contributions to F_3 and F_4 .

F_5 was evaluated by Arnold and Zhai in 1994 [29] and F_6 by Kastening and Zhai in 1995 [30]. At this order the running of the coupling constant g must already be taken into account resulting in a renormalization scale dependence in the formulas for F_5 and F_6 . The authors had to perform a resummation for the gluon propagator just as in the two previous orders and were in addition required to evaluate a large set of 2- and 3-loop diagrams. Although these calculations were originally performed in four-dimensional thermal QCD, the same results were soon derived also using another approach, namely a three-dimensional effective theory [21].

The convergence of the above free energy expansion is fairly weak at temperatures close to T_c . It is therefore essential to attempt to extend it further to the next order, where the use of an effective theory approach already becomes vital. Based on calculations in the full theory it was actually believed for a long time that beyond the g^5 term the expansion (2.7) is completely meaningless due to non-perturbative effects that enter at order g^6 [11]. The loop expansion for the free energy indeed breaks down at this order because of the chromomagnetic force, which is unscreened at scale gT and renders inapplicable the resummation needed to take into account the chromoelectric screening. For a magnetic screening mass of order g^2T it can be easily seen that diagrams of all loop orders higher than three contribute to F at order g^6 (see e.g. [5]). The problem was, however, at least partially solved in the mid 1990's by Braaten and Nieto [12, 13, 21], who used the idea of dimensional reduction to develop two effective three-dimensional theories that agree with QCD at distances larger than $1/(gT)$ and $1/(g^2T)$, respectively. These theories can be used to extract the contribution of the soft momentum scales gT and g^2T to the free energy and they thereby provide a practical method for evaluating the next term ($\mathcal{O}(g^6 \ln g)$) in (2.7). The construction of the effective theories is the subject of the next section of this thesis.

2.2 Dimensional reduction and effective QCD

The method of dimensional reduction in 3+1 -dimensional field theories is based on the observation that at sufficiently high temperatures the large distance static correlation functions can be obtained via an effective theory in three dimensions. In the following I will explain the reasoning that leads to this result.

Let us consider a generic field theory, where the masses of the different fields are of negligible magnitude in comparison with the temperature. Just as in QCD the partition function may be represented by a functional integral over the different fields, where the integrand is an exponential of the effective action with the ordinary time replaced by an imaginary one. The bosonic fields have again periodic and the fermionic fields antiperiodic boundary conditions on the interval $[0, \beta]$:

$$\phi(\mathbf{x}, \tau = \beta) = \pm \phi(\mathbf{x}, \tau = 0), \quad (2.11)$$

which leads to a Fourier representation for them in the form

$$\phi(\mathbf{x}, \tau) = T \sum_{n=-\infty}^{\infty} e^{i\omega_n \tau} \phi_n(\mathbf{x}). \quad (2.12)$$

Here the ω_n 's are the famous Matsubara frequencies, which for bosons equal $\omega_n = 2n\pi T$ and for fermions $\omega_n = (2n+1)\pi T$. The propagators of the field modes are of the form $\frac{1}{\omega_n^2 + p^2}$ showing that the nonstatic modes have effective masses proportional to T that grow very large, when the temperature approaches infinity.

There exists a decoupling theorem due to Appelquist and Carazzone [31], which states that for a renormalizable zero-temperature field theory containing fields with masses $m_1 \ll m_2$, the Green's functions with typical momentum scales $p \ll m_2$ (and distance scales $x \gg 1/m_2$) may up to corrections of order $\frac{m_1}{m_2}, \frac{p}{m_2}$ be calculated using a Lagrangian with the heavy fields removed. In the new Lagrangian the coupling constants have modified values and one furthermore needs to add new, possibly non-renormalizable interaction terms in order to reproduce the results of the old theory to a good accuracy. In the finite temperature case it is clearly the bosonic zero modes that play the role of the light fields and become the only degrees of freedom contributing to large distance correlation functions as T increases. The non-static modes are correspondingly the heavy fields and can be integrated out from the theory at high enough temperature. What happens in this process is that the τ -dependence vanishes from the Lagrangian making the theory a three-dimensional one. The new theory generally has a simpler structure than the original one due to the lack of fermions and the disappearance of tedious frequency sums from diagrammatic calculations. In addition e.g. 3d lattice simulations are considerably easier and less CPU time consuming than four-dimensional ones.

In the case of dimensionally reduced QCD the quarks have been integrated out leaving as the real degrees of freedom the $n = 0$ -term of the expansion of the gluon field

$$A_\mu^a(\mathbf{x}, \tau) = T \sum_{n=-\infty}^{\infty} e^{i\omega_n \tau} A_{\mu,n}^a(\mathbf{x}), \quad (2.13)$$

where $\omega_n = 2\pi nT$. The components of the zero-frequency mode are essentially identified with the electrostatic scalar field $A_0^a(\mathbf{x})$ and the magnetostatic gauge field $A_i^a(\mathbf{x})$ of a three-dimensional effective theory called electrostatic QCD (EQCD), which was constructed in [12] to produce the contribution of momenta of order gT to the full free energy.

Although one in principle could construct effective QCD by explicitly integrating out all field modes with nonzero Matsubara frequency, a more effective way is to simply write down the most general Lagrangian that involves the fields $A_0^a(\mathbf{x})$ and $A_i^a(\mathbf{x})$ and respects the symmetries of the theory [21]. The Lagrangian constructed in this manner contains free parameters that have to be chosen in such a way that the static correlation functions of the effective theory agree with the ones of the full theory at large distances. In the case of EQCD this distance scale is $1/(gT)$ and the Lagrangian is the super-renormalizable one of a three-dimensional 'SU(3) + adjoint Higgs' theory:

$$\mathcal{L}_{EQCD} = \frac{1}{4} F_{ij}^a F_{ij}^a + \frac{1}{2} D_i A_0^a D_i A_0^a + \frac{1}{2} m_E^2 A_0^a A_0^a + \frac{1}{8} \lambda_E (A_0^a A_0^a)^2, \quad (2.14)$$

where

$$F_{ij}^a = \partial_i A_j^a - \partial_j A_i^a + g_E f^{abc} A_i^b A_j^c. \quad (2.15)$$

A term proportional to the unit operator appearing in the EQCD Lagrangian has not been included in the definition of \mathcal{L}_{EQCD} and there are in addition higher order non-renormalizable operators involving $A_0^a(\mathbf{x})$ and $A_i^a(\mathbf{x})$ that have been suppressed here. It has been shown that at large temperatures the contribution of the higher order terms can be neglected to a good accuracy.

Using (2.14) the partition function of QCD can be expressed in the form

$$\begin{aligned} Z &= e^{-V f_E(\Lambda_E)} Z_{EQCD} \\ &= e^{-V f_E(\Lambda_E)} \int^{\Lambda_E} \mathcal{D}A_0^a \mathcal{D}A_i^b \exp \left[- \int d^3x \mathcal{L}_{EQCD} \right], \end{aligned} \quad (2.16)$$

where $f_E(\Lambda_E)$ is the coefficient of the unit operator mentioned above and an ultraviolet cut-off Λ_E has been introduced in the functional integral corresponding to the partition function of the effective theory. The reason for the appearance of Λ_E is that EQCD has been constructed to reproduce the results of the full theory only at large distances and clearly cannot be expected to be correct at arbitrarily high momenta. Λ_E plays the role of a factorization scale separating the EQCD regime from the region of high momenta that is described correctly only by full QCD.

The coefficient of the unit operator, f_E , clearly represents the explicit contribution of hard momenta of order T to the QCD free energy and can be evaluated by constructing a strict perturbation expansion for f in the original theory. The computation is performed in [21] and produces the result

$$\begin{aligned} f_E(\Lambda_E) &= -\frac{8\pi^2}{9} T^3 \left[\frac{1}{5} + \frac{21}{160} N_f - \frac{g^2(\mu)}{(4\pi)^2} \left(3 + \frac{5}{4} N_f \right) + \left(\frac{g^2(\mu)}{(4\pi)^2} \right)^2 \right. \\ &\quad \times \left(9 \left[48 \ln \frac{\Lambda_E}{4\pi T} - \frac{22}{3} \ln \frac{\mu}{4\pi T} + \frac{116}{5} + 4\gamma + \frac{148}{3} \frac{\zeta'(-1)}{\zeta(-1)} - \frac{38}{3} \frac{\zeta'(-3)}{\zeta(-3)} \right] \right. \\ &\quad \left. + \frac{3}{2} N_f \left[48 \ln \frac{\Lambda_E}{4\pi T} - \frac{47}{3} \ln \frac{\mu}{4\pi T} + \frac{367}{20} - \frac{271}{15} \ln 2 + 8\gamma + \frac{74}{3} \frac{\zeta'(-1)}{\zeta(-1)} - \frac{1}{3} \frac{\zeta'(-3)}{\zeta(-3)} \right] \right. \\ &\quad \left. \left. + \frac{1}{4} N_f^2 \left[\frac{20}{3} \ln \frac{\mu}{4\pi T} + \frac{1}{3} - \frac{88}{5} \ln 2 + 4\gamma + \frac{16}{3} \frac{\zeta'(-1)}{\zeta(-1)} - \frac{8}{3} \frac{\zeta'(-3)}{\zeta(-3)} \right] \right) \right] \\ &\quad + \mathcal{O}(g^6), \end{aligned} \quad (2.17)$$

where the order g^6 term is also in principle calculable through four-loop perturbation theory. The Euler constant γ is numerically $\gamma \approx 0.577216$ and the values of the ratio of the Riemann zeta function to its derivative required here are approximately $\frac{\zeta'(-1)}{\zeta(-1)} \approx 1.98505$ and $\frac{\zeta'(-3)}{\zeta(-3)} \approx 0.645429$. The parameter μ may be considered arbitrary, since just as in the case of (2.7), f_E can be shown to be independent of it. The expression (2.17), however, depends on the

factorization scale Λ_E explicitly and f_E therefore has a non-trivial renormalization group equation with respect to this parameter. The RGE has the solution

$$f_E(\Lambda_E) = f_E(\Lambda'_E) - \frac{3}{2\pi^2} g_E^2 m_E^2 \ln \frac{\Lambda_E}{\Lambda'_E}. \quad (2.18)$$

The contribution of lower momentum scales to different observables of thermal QCD can be calculated in the effective theory, where one needs expressions for the coupling constants g_E , m_E^2 and λ_E . The matching of static correlation functions of EQCD to those of original QCD at distances of order $1/(gT)$ and larger leads to expansions for these parameters as functions of T , Λ_E and g and implies that besides through f_E , the contribution of the energy scale T to the original free energy enters through them. In [21] the quantities needed in the matching process are evaluated as strict perturbation expansions in g , and the same infrared cut-off is applied both to EQCD and to full QCD. This is not the physically correct way of dealing with the infrared divergencies of the theory since one is then totally neglecting the screening effects. It however leads to correct values for the EQCD parameters, which is due to their leading contributions coming from the hard momentum scales. In the following I will briefly review the calculation of the parameters performed in [21] and [22], where relative errors are of order g^4 .

The three-dimensional gauge coupling g_E may at lowest order be directly read off from the QCD Lagrangian, where the gluon fields have been expressed in terms of the EQCD fields using (2.13). Higher order corrections can be obtained either by matching scattering amplitudes in EQCD and full QCD or by calculating the contribution of the neglected field modes to the correlation function of A_i^a and A_j^b . One obtains [22]

$$g_E^2 = g^2(\mu) T \left[1 + \frac{g^2(\mu)}{(4\pi)^2} \left(\frac{2}{3} (33 - 2N_f) \ln \frac{\mu}{\mu_T} - \frac{8}{3} N_f \ln 2 + 1 \right) \right], \quad (2.19)$$

where $\mu_T = 4\pi e^{-\gamma} T$. As the other EQCD parameters, g_E is scale independent to order g^6 : $\mu \frac{\partial g_E^2}{\partial \mu} = \mathcal{O}(g^6)$. Using (2.6) one may therefore express (2.19) in terms of any scale and μ may be regarded as an arbitrary mass parameter. The coupling is independent of the factorization scale Λ_E .

The mass parameter m_E , which is the contribution of scale T to the chromoelectric screening mass m_{el} , can at two-loop level be obtained by matching EQCD and QCD results for the strict perturbation expansion of m_{el} [21]. Just as the works of Kapusta and Toimela [27, 28], also this calculation involves the evaluation of the 00-component of the gluon self-energy at $p_0 = 0$ in full thermal QCD. Following the g_E^2 -calculation one may express m_E^2 in terms of an unspecified scale μ instead of the scale of dimensional regularization. This leads to:

$$m_E^2 = \left(1 + \frac{1}{6} N_f \right) g^2(\mu) T^2 \times \left[1 + \frac{g^2(\mu)}{(4\pi)^2} \left(\frac{2}{3} (33 - 2N_f) \ln \frac{\mu}{\mu_T} - \frac{8}{3} N_f \ln 2 + \frac{90 + 2N_f^2 + 3N_f}{18 + 3N_f} \right) \right]. \quad (2.20)$$

The dependence of (2.20) on Λ_E is only weak:

$$\Lambda_E \frac{\partial m_E^2}{\partial \Lambda_E} = \frac{2 \cdot 8 \cdot (3g_E^2 - \lambda_E) \lambda_E}{(4\pi)^2} \quad (2.21)$$

In order to evaluate λ_E one needs the two-loop effective potential of the full four-dimensional theory. It is calculated in [32] and leads to the result [22]:

$$\begin{aligned} \lambda_E &= \left(3 - \frac{1}{3} N_f\right) \frac{g^4(\mu) T}{8\pi^2} \\ &\times \left[1 + 2 \frac{g^2(\mu)}{(4\pi)^2} \left(\frac{2}{3} (33 - 2N_f) \ln \frac{\mu}{\mu_T} - \left(\frac{8}{3} \ln 2 - \frac{2}{3}\right) N_f + \frac{7/2 - 23N_f/18}{1 - N_f/9}\right)\right], \end{aligned} \quad (2.22)$$

where μ is arbitrary as before. Clearly λ_E is independent of the factorization scale.

Using the above expressions for the different parameters of the EQCD Lagrangian one is now able to e.g. evaluate the free energy of the full theory to order g^5 [21]. Since the ultimate purpose is, however, to calculate f to an even higher order, one needs to construct another effective theory, magnetostatic QCD (MQCD) [12], in order to further separate the contributions of the scales gT and g^2T . This is achieved by integrating out the electrostatic field $A_0^a(\mathbf{x})$ and leads to a Lagrangian for MQCD that corresponds to a three-dimensional pure gauge theory:

$$\mathcal{L}_{MQCD} = \frac{1}{4} F_{ij}^a F_{ij}^a. \quad (2.23)$$

Here F_{ij}^a is as in (2.15) but with g_E replaced by g_M , the MQCD gauge coupling constant. Just as in (2.14) a term proportional to the unit operator has been left out from the definition of \mathcal{L}_{MQCD} and higher order operators have been suppressed.

The partition function of MQCD is defined in close analogy with the construction of Z_{EQCD} in (2.16):

$$\begin{aligned} Z_{EQCD} &= e^{-V f_M(\Lambda_E, \Lambda_M)} Z_{MQCD} \\ &= e^{-V f_M(\Lambda_E, \Lambda_M)} \int^{\Lambda_M} \mathcal{D}A_i^a \exp \left[- \int d^3x \mathcal{L}_{MQCD} \right]. \end{aligned} \quad (2.24)$$

Here $f_M(\Lambda_E, \Lambda_M)$ is now the coefficient of the unit operator of the MQCD Lagrangian and the ultraviolet cut-off Λ_M has been introduced to explicitly separate the scales gT and g^2T . The coefficient f_M as well as the coupling g_M can be obtained in terms of the EQCD parameters by matching MQCD and EQCD calculations. The first one has been evaluated to three loops in [21] with the result being

$$\begin{aligned} f_M(\Lambda_E) &= -\frac{2}{3\pi} m_E^3 \left[1 - \frac{3g_E^2}{4\pi m_E} \left(\frac{9}{4} + 3 \ln \frac{\Lambda_E}{2m_E} \right) \right. \\ &\quad \left. + \left(\frac{3g_E^2}{4\pi m_E} \right)^2 \left(-\frac{89}{8} - \frac{\pi^2}{2} + \frac{11}{2} \ln 2 \right) \right]. \end{aligned} \quad (2.25)$$

Using (2.16) and (2.24) one may now write down the free energy of full QCD in terms of the effective theory quantities f_E , f_M and Z_{MQCD} [21]:

$$f = T \left[f_E(T, g; \Lambda_E) + f_M(m_E^2, g_E, \lambda_E; \Lambda_E, \Lambda_M) - \frac{1}{V} \ln Z_{MQCD}(g_M; \Lambda_M) \right]. \quad (2.26)$$

Here the effects of the different momentum scales are clearly visible. The coefficient f_E contains the contribution of large momenta of order T to the free energy and can be calculated in full thermal QCD as a power series expansion in g^2 (2.17) starting at order g^0 . The second part, f_M , represents the scale gT in the calculation and is obtained as a perturbative expansion in EQCD (2.25) with the leading term being proportional to m_E^3 . It therefore contributes to the full free energy starting at order g^3 . The last term of (2.26) contains the logarithm of Z_{MQCD} and cannot be obtained perturbatively. Lattice simulations are anyway expected to lead to a result for it, where the leading contribution is of order $g^6 \ln g$.

The role of the different momentum cut-offs used in the above is now obvious, too. There are altogether four scales that have appeared: the renormalization scale, the factorization scales Λ_E and Λ_M and in addition the infrared scale Λ_{QCD} . As explained before, the last one is an integration constant coming from the RGE of the gauge coupling g and corresponds to the logarithmic divergence of (2.6) at small momenta. It can be viewed as the natural infrared cut-off of full QCD and it provides a scale for all considerations here. Λ_M , on the other hand, merely separates the MQCD and EQCD regions being at the same time both the ultraviolet -cut off of MQCD and the IR -cut off of EQCD. The role of Λ_E is similar to that as it acts as the scale separating EQCD from the full theory. Finally, the momentum parameter corresponding to the renormalization of the original theory is an ultraviolet one of order $1/(\text{fm})$ but has no actual physical meaning.

2.3 The three-dimensional free energy

Ever since the g^5 term of the free energy expansion (2.7) was first obtained, the both theoretically and technically very challenging task of further improving the validity of the series has been tackled by various people (see e.g. [6, 14, 33]). The evaluation of the next order term was first outlined in [21] by Braaten and Nieto, who took advantage of the separation of scales T , gT and g^2T in (2.26) provided by their effective theories EQCD and MQCD. The contribution to the order g^6 term from momenta of order T was shown to be available through a four-loop calculation of f_E in the full four-dimensional theory and an $\mathcal{O}(\epsilon)$ evaluation of the constants g_E^2 and λ_E . In order to obtain the gT part one must, on the other hand, evaluate f_M as a perturbative expansion in EQCD up to four-loop order and there use the order g^4 result (2.19) for the parameter g_E^2 . Finally the authors argued that the contribution from the magnetic sector can be calculated by determining the coefficients a and b in the expansion $-\ln Z_{EQCD}/V = (a + b \ln \frac{\Lambda_M}{g_M^2})g_M^6$. According to them a is non-perturbative and may only be obtained by means of lattice simulations in a three-dimensional pure gauge theory, whereas b can be calculated analytically by simply evaluating four-loop MQCD vacuum diagrams. It has, however, been shown in [22] that such a straightforward picture has an inconsistency in the construction of MQCD, since it is only at unreasonably high temperatures that the

magnetic sector contributions to the free energy of the three-dimensional theory can be seen to be small in comparison with the electric ones.

Kajantie, Laine, Rummukainen and Schröder have recently applied methods similar to the ones described above to combine analytic calculations with lattice Monte Carlo simulations in order to extract the contributions of the different energy scales to f . In particular they have built in [14] a new method for resumming the long-distance contributions to the free energy of a three-dimensional effective QCD. This work is based on the papers [22], where a 3d 'SU(N) + adjoint Higgs' theory with a Lagrangian corresponding to (2.14) is studied at high temperatures.

In [22] the authors define dimensionless parameters $x = \lambda_E/g_E^2$ and $y = m_E^2 (\bar{\mu}_3 = g_E^2)/g_E^4$ ($\bar{\mu}_3$ being the $\overline{\text{MS}}$ dimensional regularization scale in three dimensions) and show that choosing such renormalization scales for the effective theory parameters that their next-to-leading-order corrections vanish leads to:

$$\begin{aligned} g_E^2 &= \frac{24\pi^2}{33 - 2N_f} \frac{1}{\ln(\mu_g \mu_T / \Lambda_{\overline{\text{MS}}})} T, \\ x &= \frac{9 - N_f}{33 - 2N_f} \frac{1}{\ln(\mu_x \mu_T / \Lambda_{\overline{\text{MS}}})} \quad \text{and} \\ y &= \frac{(9 - N_f)(6 + N_f)}{144\pi^2 x} + \frac{486 - 33N_f - 11N_f^2 - 2N_f^3}{96(9 - N_f)\pi^2} + \mathcal{O}(x), \end{aligned} \quad (2.27)$$

where N has been set equal to three,

$$\mu_i = \exp\left(\frac{-3c_i + 4N_f \ln 4}{66 - 4N_f}\right), \quad c_g = 1, \quad c_x = \frac{4}{3}N_f + \frac{54 - 22N_f}{9 - N_f}, \quad \Lambda_{\overline{\text{MS}}} \sim T_C \quad (2.28)$$

and μ_T is as in (2.19). With help of equations (2.19)-(2.22) it can be observed that to leading order $x \sim g^2$ and $y \sim 1/g^2$.

Using the parameters x and y Kajantie et al. write in [14] the pressure ($= -f$) of full QCD in the form

$$\begin{aligned} p(T) &= p_0(T) \left[1 - \frac{5}{2}x \right. \\ &\quad \left. + \frac{45}{8\pi^2} \left(\frac{g_E^2}{T}\right)^3 \left(\frac{3}{2\pi^2} y \left(\ln \frac{\bar{\mu}_{3d}}{T} + \delta\right) - \mathcal{F}_{\overline{\text{MS}}}(x, y)\right) + \mathcal{O}(g^6) \right], \end{aligned} \quad (2.29)$$

where $\bar{\mu}_{3d}$ may be identified with Λ_E and δ is an analytically known constant of negligible magnitude that can be obtained from (2.17). The factor $p_0(T) = \frac{8\pi^2 T^4}{45} \left(1 + \frac{21}{32}N_f\right)$ represents the ideal gas result discussed above (the term F_0 in (2.7)), and when written in terms of the full QCD gauge coupling g , the first three terms of (2.29) have perturbative expansions starting respectively at orders g^0 , g^2 and g^4 . The term $\mathcal{F}_{\overline{\text{MS}}}(x, y)$, which essentially equals the previous $g_E^6 f_M$, is the dimensionless free energy of three-dimensional QCD and represents

the contribution of momenta of order gT and smaller to the original f . The $\mathcal{O}(g^6)$ error in (2.29) originates from higher momentum scales and is therefore not connected to $\mathcal{F}_{\overline{\text{MS}}}$.

In the new notation $\mathcal{F}_{\overline{\text{MS}}}(x, y)$ can be written as [14]

$$\begin{aligned} \frac{\mathcal{F}_{\overline{\text{MS}}}(x, y)}{8} &= y^2 \left(-\frac{1}{4\pi\sqrt{y}} \frac{1}{3} + \frac{1}{(4\pi\sqrt{y})^2} \left[\frac{9}{4} - \frac{3}{2} \ln 4y + 3 \ln \frac{\bar{\mu}_{3d}}{g_E^2} + \frac{5}{2} x \right] \right. \\ &\quad + \frac{1}{(4\pi\sqrt{y})^3} \left[\frac{267}{8} + \frac{3\pi^2}{2} - \frac{33}{2} \ln 2 - 15 \left(\frac{1}{2} - \ln 4y \right) x \right. \\ &\quad \left. \left. + 5 \left(\frac{1}{2} - \ln 16y \right) x^2 \right] \right) + \frac{\Delta\mathcal{F}_{\overline{\text{MS}}}(x, y)}{8}, \end{aligned} \quad (2.30)$$

where the expansion parameters are now x and $1/(4\pi\sqrt{y})$. This expression is equivalent to (2.25) except that here the self-coupling of the A_0^a fields has been taken into account (x has not been set equal to zero). Apart from the other x -dependent terms it is clearly $\Delta\mathcal{F}_{\overline{\text{MS}}}(x, y)$ that represents the previously undetermined part of f .

The approach of [14] is to differentiate $\Delta\mathcal{F}_{\overline{\text{MS}}}(x, y)$ with respect to x and y , calculate the derivatives by means of lattice studies and then finally numerically integrate the result back in the form

$$\begin{aligned} \Delta\mathcal{F}_{\overline{\text{MS}}}(x, y) &= \Delta\mathcal{F}_{\overline{\text{MS}}}(x_0, y_0) \\ &\quad + \int_{y_0}^y dy \left(\frac{\partial\Delta\mathcal{F}_{\overline{\text{MS}}}(x(y), y)}{\partial y} + \frac{dx(y)}{dy} \frac{\partial\Delta\mathcal{F}_{\overline{\text{MS}}}(x(y), y)}{\partial x} \right). \end{aligned} \quad (2.31)$$

The partial derivatives can easily be related to expectation values of different operators using the path integral representation of Z_{EQCD} (2.16). In fact the two terms in the integrand of (2.31) are respectively the differences of the quadratic and quartic A_0 condensates and their perturbative results in $\overline{\text{MS}}$ scheme, and the nonperturbative values can be obtained from lattice ones through multi-loop calculations both in ordinary and lattice perturbation theory. For the y -derivative the equation relating it to the condensates is

$$\frac{\partial\Delta\mathcal{F}_{\overline{\text{MS}}}}{\partial y} = \left\langle \frac{A_0^a A_0^a}{2g_E^2} \right\rangle_{\overline{\text{MS}}} - \left\langle \frac{A_0^a A_0^a}{2g_E^2} \right\rangle_{\overline{\text{MS}}, \text{ pert.}}, \quad (2.32)$$

where the perturbative result can be directly read off from (2.30). The difference as measured with different lattice spacings is shown in figure 2.1.

The integration constant in equation (2.31), $\Delta\mathcal{F}_{\overline{\text{MS}}}(x_0, y_0)$, is on the other hand expected to have the form

$$\Delta\mathcal{F}_{\overline{\text{MS}}}(x_0, y_0) = \frac{8 \cdot 3^3}{(4\pi)^4} e_0 \left(1 + \mathcal{O} \left(\frac{x_0}{3}, \frac{3}{4\pi y_0^{1/2}} \right) \right), \quad (2.33)$$

where e_0 is an unknown parameter. If $\Delta\mathcal{F}_{\overline{\text{MS}}}(x_0, y_0)$ is fixed at a temperature $T_0 = 10^{11} \Lambda_{\overline{\text{MS}}}$, where $x_0 = 0.01$ and $y_0 = 3.86$, the terms not explicitly shown in (2.33) can be neglected

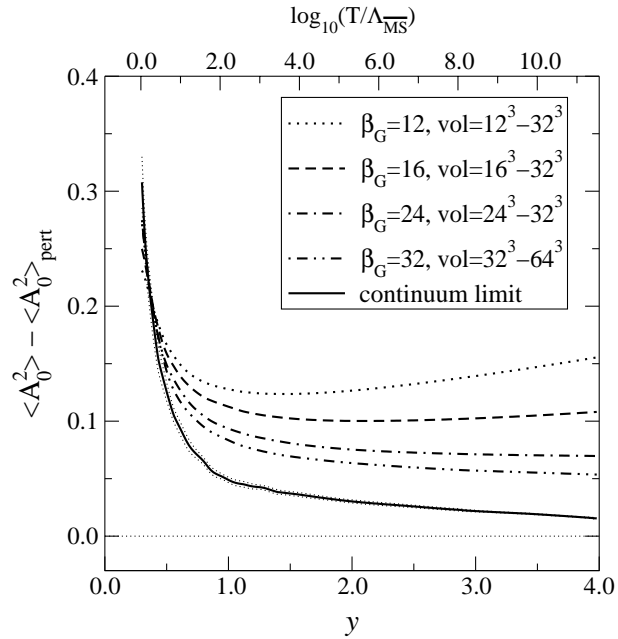


Figure 2.1: Equation (2.32) as measured using Monte Carlo simulations with different lattice spacings a . Here $\beta_G = 6/(g_E^2 a)$ and the continuum limit naturally corresponds to $\beta_G \rightarrow \infty$. The figure is taken from [14].

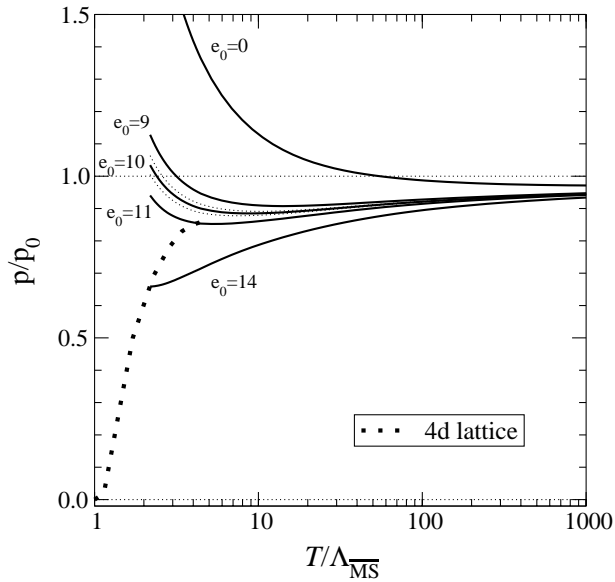


Figure 2.2: The behaviour of the QCD pressure as a function of e_0 [14]. For $e_0 = 10$ statistical errors are indicated. The lattice data is from [9].

and knowing the value of e_0 suffices. As can be seen from figure 2.2, at temperatures below $(20 - 50)T_c$ the behaviour of the perturbative pressure depends strongly on e_0 , which is presently being treated as a free parameter. The figure is taken from [14], where the authors note that the expansions computed by them are reliable only when $T \geq 5T_c$ but that by taking into account also the quartic condensate neglected so far, one will in principle be able to reduce the lower limit down to $2T_c$.

The next logical step in the perturbative determination of the free energy at temperatures near T_c would seem to be the explicit evaluation of e_0 through extensive lattice studies. This is, however, a very complicated task requiring e.g. four-loop calculations in ordinary and lattice perturbation theory and is not presently being pursued. The complexity of the problem is not surprising at all, since one easily sees from (2.29)-(2.33) that e_0 represents the contribution of the infamous g^6 term to the original free energy expansion. As mentioned earlier, it was shown by Linde already in 1980 [11] that this part is entirely nonperturbative, since it gets contributions from full QCD diagrams of all loop orders greater than three. Regarding e_0 still as a free parameter it is however notable that for values $e_0 = 10.0 \pm 2.0$, as Kajantie et al. estimate, the above calculations produce a convincing agreement between the perturbative results and four-dimensional lattice data (figure 2.2). The setup of [14] has therefore produced a theoretical framework, which has the capacity of explaining the behaviour of the free energy on a temperature range from a few times T_c all the way to infinity, while taking the long-distance contributions systematically into account. Using this approach one is in particular able to see, why the long-distance effects do not necessarily cause a large deviation between the measured pressure and its g^5 -result (figure 2.3). In comparison with previous results and other approaches, e.g. [6, 33], this is a significant improvement.

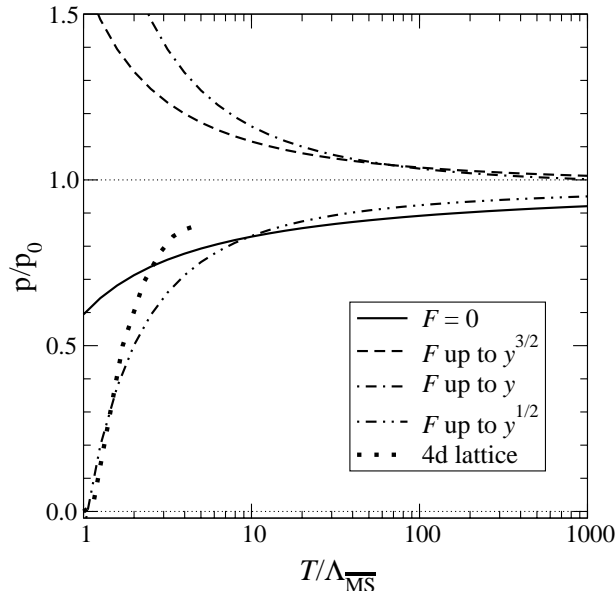


Figure 2.3: The perturbative pressure of (2.29) as taken from [14], where different orders of the expansion (2.30) have been taken into account.

2.4 The skeleton expansion

Determining the loop expansion of the free energy in a three-dimensional 'SU(3) + adjoint scalar' theory clearly plays an essential role in the computation of the perturbative free energy of full finite temperature QCD. At four-loop level the number of different diagrams contributing to $\mathcal{F}_{\overline{\text{MS}}}$ is already considerable and some method is needed for organizing and grouping them. This is provided by the so called skeleton expansion [34, 35], which was used in [15] for writing down the loop expansion of the QCD free energy in terms of two-particle irreducible diagrams (skeletons) and ring diagrams containing self energy insertions. It was further shown in [15] that the self energies needed in the computation can be straightforwardly obtained from lower order skeletons. Below I shall briefly introduce this method and explicitly list all skeleton diagrams up to four-loop order that are needed in the calculation of the free energy of the effective theory and that eventually lead to the scalar integrals of the later chapters.

Let us first study the free energy of a generic field theory along the lines of [15] and denote the full propagators of the different fields by D_i , the free ones by Δ_i and the proper self-energies by Π_i . The starting point of the skeleton approach is a formula derived in [34, 35], which gives the free energy in terms of a function $\Phi[D]$ containing all vacuum skeletons:





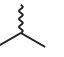



$$F[D] = \sum_i c_i \left(\text{Tr} \ln D_i^{-1} + \text{Tr} \Pi_i[D] D_i \right) - \Phi[D]. \quad (2.34)$$

Here the sum goes over bosons and fermions with c_i being 1/2 for bosons and -1 for fermions. The equation can be modified by writing the right hand side in a form containing only free propagators, which is an essential simplification from the point of view of practical calculations. Denoting the terms in the loop expansion of Φ by Φ_n and expanding the D_i 's in terms of self-energies, the authors of [15] obtain:

$$\begin{aligned} -F &= -F_0 + \Phi_2[\Delta] \\ &+ \left(\Phi_3[\Delta] + \sum_i c_i \left(\frac{1}{2} \textcircled{1} \right) \right) \\ &+ \left(\Phi_4[\Delta] + \sum_i c_i \left(\frac{1}{3} \textcircled{1} \textcircled{1} \textcircled{1} + \textcircled{1} \textcircled{2} + \frac{1}{2} \textcircled{1} \textcircled{2} \right) \right) \\ &+ \left(\Phi_5[\Delta] + \sum_i c_i \left(\frac{1}{4} \textcircled{1} \textcircled{1} \textcircled{1} \textcircled{1} + \textcircled{1} \textcircled{2} \textcircled{1} + \frac{1}{2} \textcircled{1} \textcircled{2} \textcircled{1} \right. \right. \\ &\left. \left. + \frac{1}{2} \textcircled{2} \textcircled{2} + \frac{1}{2} \textcircled{2} \textcircled{2} + \textcircled{1} \textcircled{3} + \frac{1}{2} \textcircled{1} \textcircled{3} + \frac{1}{3} \textcircled{1} \textcircled{3} \right) \right), \end{aligned} \quad (2.35)$$

where the circles and squares are respectively irreducible and reducible self-energies and the loop order is indicated by the number inside. As mentioned above, all self-energies are available through the Φ_n 's.

Since the ring diagrams are generally considerably easier to evaluate than the skeleton ones it can be seen from (2.35) that what is most urgently needed in order to obtain the free energy to different orders are the terms Φ_n that originate from the loop expansion of Φ . In

the case of the three-dimensional QCD containing as particles A_i^a -gauge bosons , A_0^a -scalars  and ghosts , and as vertices , , ,  and , one obtains [15]:

$$\Phi_2 = \frac{1}{8} \text{diagram} + \frac{1}{12} \text{diagram} - \frac{1}{2} \text{diagram} + \frac{1}{4} \text{diagram} + \frac{1}{4} \text{diagram} + \frac{1}{8} \text{diagram}, \quad (2.36)$$

$$\begin{aligned} \Phi_3 = & \frac{1}{24} \text{diagram} - \frac{1}{3} \text{diagram} - \frac{1}{4} \text{diagram} + \frac{1}{8} \text{diagram} + \frac{1}{48} \text{diagram} + \frac{1}{6} \text{diagram} + \frac{1}{8} \text{diagram} \\ & + \frac{1}{2} \text{diagram} + \frac{1}{4} \text{diagram} + \frac{1}{8} \text{diagram} + \frac{1}{8} \text{diagram} + \frac{1}{48} \text{diagram}, \end{aligned} \quad (2.37)$$

$$\begin{aligned} \Phi_4 = & \frac{1}{72} \text{diagram} - \frac{1}{4} \text{diagram} - \frac{1}{6} \text{diagram} + \frac{1}{12} \text{diagram} - \frac{1}{2} \text{diagram} - \frac{1}{2} \text{diagram} \\ & - 1 \text{diagram} - \frac{1}{3} \text{diagram} + \frac{1}{6} \text{diagram} + \frac{1}{6} \text{diagram} + \frac{1}{8} \text{diagram} - \frac{1}{4} \text{diagram} \\ & + \frac{1}{4} \text{diagram} - \frac{1}{2} \text{diagram} + \frac{1}{8} \text{diagram} + \frac{1}{8} \text{diagram} + \frac{1}{16} \text{diagram} + \frac{1}{48} \text{diagram} \\ & + \frac{1}{8} \text{diagram} + \frac{1}{12} \text{diagram} - \frac{1}{3} \text{diagram} + \frac{1}{4} \text{diagram} + \frac{1}{4} \text{diagram} + \frac{1}{2} \text{diagram} \\ & + \frac{1}{6} \text{diagram} + \frac{1}{12} \text{diagram} + \frac{1}{2} \text{diagram} + \frac{1}{2} \text{diagram} + \frac{1}{2} \text{diagram} + \frac{1}{8} \text{diagram} + \frac{1}{4} \text{diagram} \\ & + \frac{1}{4} \text{diagram} - \frac{1}{2} \text{diagram} + \frac{1}{4} \text{diagram} + \frac{1}{4} \text{diagram} + \frac{1}{4} \text{diagram} + \frac{1}{4} \text{diagram} + 1 \text{diagram} + 1 \text{diagram} \\ & + \frac{1}{4} \text{diagram} + \frac{1}{8} \text{diagram} + \frac{1}{2} \text{diagram} + \frac{1}{2} \text{diagram} + \frac{1}{8} \text{diagram} + \frac{1}{4} \text{diagram} \\ & + \frac{1}{8} \text{diagram} + \frac{1}{2} \text{diagram} + \frac{1}{2} \text{diagram} + \frac{1}{8} \text{diagram} + \frac{1}{16} \text{diagram} + \frac{1}{2} \text{diagram} + \frac{1}{16} \text{diagram} \\ & + \frac{1}{16} \text{diagram} + \frac{1}{6} \text{diagram} + \frac{1}{4} \text{diagram} + \frac{1}{4} \text{diagram} + \frac{1}{4} \text{diagram} + \frac{1}{4} \text{diagram} + \frac{1}{2} \text{diagram} \\ & + \frac{1}{8} \text{diagram} + \frac{1}{16} \text{diagram} + \frac{1}{8} \text{diagram} + \frac{1}{16} \text{diagram} + \frac{1}{48} \text{diagram}. \end{aligned} \quad (2.38)$$

The evaluation of the loop expansion of $\mathcal{F}_{\overline{\text{MS}}}$ to different orders has here been reduced to the laborious task of calculating well-defined but large sets of Feynman diagrams in three dimensions. The diagrams contain propagators and vertices of gauge bosons, ghosts and massive scalars making their evaluation technically very difficult. A software designed for the symbolic manipulation of mathematical expressions such as FORM [16] can be used as a powerful tool in further reducing (2.36)-(2.38) into a set of scalar diagrams containing powers and scalar products of loop momenta in the numerators of their integrands. The evaluation of these scalar integrals remains, however, still to be done.

The remaining of this thesis is devoted to the calculation of a subset of the four-loop scalar diagrams mentioned above, namely all scalar graphs originating from Φ_4 but having no contributions in the numerators of the corresponding integrands. The different topologies

found from (2.38) constitute the diagrams of chapters 4 and 6, but in addition to this I will in chapter 5 evaluate two four-loop diagrams containing five-vertices. They are needed in lattice perturbation theory, where the Φ_n 's get additional contributions with the following topologies [15] (these diagrams are for a generic field theory):

$$\Phi_3 \Big|_{\text{lat}} = \frac{1}{12} \text{Diagram 1} + \frac{1}{48} \text{Diagram 2}, \quad (2.39)$$

$$\begin{aligned} \Phi_4 \Big|_{\text{lat}} = & \frac{1}{8} \text{Diagram 3} + \frac{1}{12} \text{Diagram 4} + \frac{1}{240} \text{Diagram 5} + \frac{1}{12} \text{Diagram 6} + \frac{1}{8} \text{Diagram 7} + \frac{1}{16} \text{Diagram 8} \\ & + \frac{1}{48} \text{Diagram 9} + \frac{1}{72} \text{Diagram 10} + \frac{1}{48} \text{Diagram 11} + \frac{1}{48} \text{Diagram 12} + \frac{1}{384} \text{Diagram 13} \end{aligned} \quad (2.40)$$

As scalar diagrams the non-trivial ones in the above expression for $\Phi_4 \Big|_{\text{lat}}$ are clearly the second and third diagrams, since the first is computationally equivalent to the N topology (see chapter 3) appearing already in (2.38) and the others factorize into products of lower-order integrals.

Chapter 3

Evaluation of scalar diagrams in three dimensions

The treatment of the four-loop diagrams of this thesis will be somewhat analogous to the three-loop considerations of Rajantie in [20]. Due to the nature of the effective three-dimensional QCD, the Feynman rules applied can be chosen to be extremely simple. Each solid line with momentum p will be represented by the propagator $\Delta(p) \equiv 1/(p^2 + m_a^2)$ and in all vertices momentum is conserved but no additional vertex function or coupling constant is inserted. The metric is Euclidean and the integrations will be performed in $3 - 2\epsilon$ -dimensions in order to regularize ultraviolet divergencies; no IR-singularities will arise, since the propagators are massive. The integration measure chosen here is the $\overline{\text{MS}}$ one:

$$\int_p = \frac{4\pi m^{1+2\epsilon}}{(\pi e^{-\gamma})^\epsilon} \int \frac{d^{3-2\epsilon}p}{(2\pi)^{3-2\epsilon}}, \quad (3.1)$$

where m is an arbitrary mass parameter.

In the calculations I will use arbitrary propagator masses whenever possible, which is essential not only from point of view of generality but also since in certain applications of the effective QCD different kinds of mass configurations may appear. When a scalar integral has been evaluated with arbitrary masses, one is in addition able to instantly obtain results for diagrams with the same topology but with propagators raised to arbitrary powers through simple differentiation of the initial result. There furthermore exist analytic relations such as the equation 1 of [20], which relates $n-1$ -loop 2-point functions to n -loop vacuum diagrams, that may be applied to the results of this thesis and that naturally are considerably more useful when arbitrary propagator masses are used.

To illustrate the above conventions let us now consider the simplest possible vacuum scalar diagram in three dimensions, which is nothing but the single bubble:

$$\textcircled{a} \equiv I(m_a) \equiv \int_p \frac{1}{p^2 + m_a^2}. \quad (3.2)$$

Performing the integration using standard formulae results in

$$I(m_a) = \frac{4\pi m^{1+2\epsilon}}{(\pi e^{-\gamma})^\epsilon} \frac{2\pi^{3/2-\epsilon}}{\Gamma(3/2-\epsilon)} \int_0^\infty \frac{dp}{(2\pi)^{3-2\epsilon}} p^{-2\epsilon} \left(1 - \frac{m_a^2}{p^2 + m_a^2}\right)$$

$$\begin{aligned}
&= -\frac{m^{1+2\epsilon}m_a^{1-2\epsilon}e^{\gamma\epsilon}}{2^{1-2\epsilon}\sqrt{\pi}\Gamma(3/2-\epsilon)}\int_0^\infty dx\frac{x^{-1/2-\epsilon}}{x+1} \\
&= -\frac{m^{1+2\epsilon}m_a^{1-2\epsilon}e^{\gamma\epsilon}}{2^{1-2\epsilon}\sqrt{\pi}\Gamma(3/2-\epsilon)}\frac{\Gamma(1/2+\epsilon)\Gamma(1/2-\epsilon)}{\Gamma(1)} \\
&= -\frac{1}{1-2\epsilon}\frac{\Gamma(1/2+\epsilon)}{\Gamma(1/2)}\left(\frac{4e^\gamma m^2}{m_a^2}\right)^\epsilon mm_a \\
&= -(1+2\epsilon)(1-\epsilon(\gamma+2\ln 2))\left(1+\epsilon\left(2\ln 2+\gamma+2\ln\frac{m}{m_a}\right)\right)mm_a \\
&= -mm_a\left(1+2\epsilon\left(1+\ln\frac{m}{m_a}\right)\right)+\mathcal{O}(\epsilon^2), \tag{3.3}
\end{aligned}$$

where the vanishing of dimensionless integrals under dimensional regularization has been used along with the known value of the function $\psi(z)\equiv\frac{\Gamma'(z)}{\Gamma(z)}$ at $z=1/2$: $\psi(1/2)=-\gamma-2\ln 2$. If one were interested in the value of (3.2) with the propagator squared, a simple differentiation with respect to $-m_a^2$ would produce the correct result. As will be seen later, calculations to higher loop orders are in many ways analogous, but they often require the use of more sophisticated integration methods. In the case of convergent diagrams I will hereafter set $\epsilon=0$ already in the beginning of the calculation and will actually not evaluate the $\mathcal{O}(\epsilon)$ part of any diagram. Each result is therefore to be viewed as being of order ϵ^0 .

The set of diagrams considered in this thesis is printed in figure 3.1. In the following I shall denote the value of each diagram as a function of its propagator masses as $I_i(m_{i_1},\dots,m_{i_n})$, where the ordering of the masses can in each case be found upon comparison with the diagrams below, which correspond to $I_i(m_1,\dots,m_n)$. This canonical expression will from now on be abbreviated simply by I_i . For a few diagrams I will also use specific names given below, the origin of which is obvious from the figure. It should, however, be kept in mind that the illustrations of the different topologies in fig 3.1 are by far not unique: e.g. the 'wheel' diagram can easily be seen to be equivalent to the letter 'A' inside a circle.

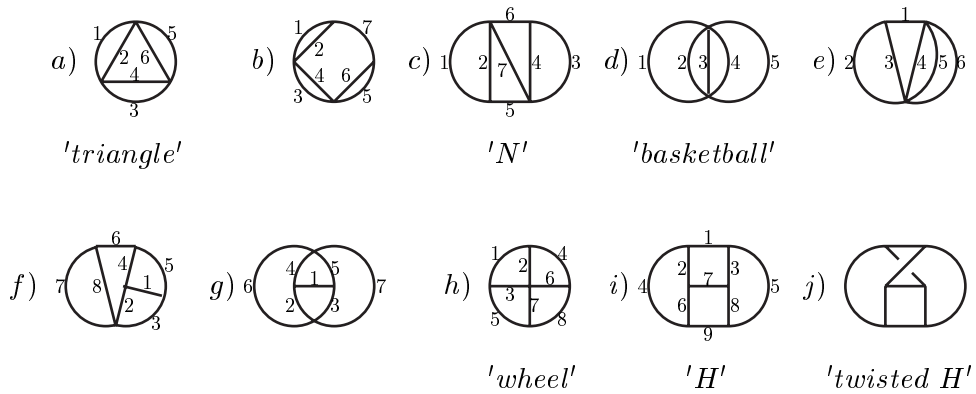


Figure 3.1: Diagrams evaluated in this thesis.

Chapter 4

Diagrams evaluated in momentum space

4.1 Diagram *a*

The triangle diagram has been studied both in three and four dimensions [13, 36] with the result that its divergent part has been found. As will be seen here, the finite term of the three-dimensional case is also available through straightforward calculations.

Using the Feynman rules stated above the value of the diagram can be seen to correspond to the four-fold momentum integral

$$I_a \equiv \int_p \int_q \int_r \int_s \frac{1}{p^2 + m_1^2} \frac{1}{(p-s)^2 + m_2^2} \times \frac{1}{q^2 + m_3^2} \frac{1}{(q-s)^2 + m_4^2} \frac{1}{r^2 + m_5^2} \frac{1}{(r-s)^2 + m_6^2}. \quad (4.1)$$

Counting the powers of momenta in the numerator and denominator one easily observes that this expression indeed diverges in three dimensions necessitating the use of $d = 3 - 2\epsilon$.

The diagram contains three identical one-loop subdiagrams in the form of a two-point function having the representation (see e.g. [37]):

$$\begin{aligned} \text{Diagram } a &\equiv \int_q \frac{1}{q^2 + m_1^2} \frac{1}{(q-p)^2 + m_2^2} \\ &= \frac{e^{\gamma\epsilon} m^{1+2\epsilon} \Gamma(1/2 + \epsilon)}{2^{1-2\epsilon} \sqrt{\pi} (p^2)^{1/2+\epsilon}} \int_0^1 dx \frac{1}{(x(1-x) + (xm_1^2 + (1-x)m_2^2) / p^2)^{1/2+\epsilon}} \\ &\equiv \frac{e^{\gamma\epsilon} m^{1+2\epsilon} \Gamma(1/2 + \epsilon)}{2^{1-2\epsilon} \sqrt{\pi} (p^2)^{1/2+\epsilon}} B(p, m_1, m_2, \epsilon), \end{aligned} \quad (4.2)$$

where the function B possesses the properties

$$\lim_{y \rightarrow \infty} B(y, \alpha_1, \alpha_2, \epsilon) = \frac{2^{2\epsilon} \sqrt{\pi} \Gamma(1/2 - \epsilon)}{\Gamma(1 - \epsilon)} \quad (4.3)$$

$$B(y, \alpha_1, \alpha_2, 0) = 2 \arctan\left(\frac{y}{\alpha_1 + \alpha_2}\right). \quad (4.4)$$

The use of this result simplifies the evaluation of the original integral significantly. The angular part of (4.1) becomes trivial due to (4.2) and one is lead to a one-dimensional integral representation for the triangle diagram:

$$I_a = 2^{-3} \pi^{-2} m^4 (4e^\gamma)^{4\epsilon} \frac{\Gamma(1/2 + \epsilon)^3}{\Gamma(3/2 - \epsilon)} \times \int_0^\infty dy y^{-1-8\epsilon} B\left(y, \frac{m_1}{m}, \frac{m_2}{m}, \epsilon\right) B\left(y, \frac{m_3}{m}, \frac{m_4}{m}, \epsilon\right) B\left(y, \frac{m_5}{m}, \frac{m_6}{m}, \epsilon\right). \quad (4.5)$$

The divergence of the initial diagram is here still contained in the integral, whose expression has a pole in ϵ . That can, however, be conveniently separated by performing a partial integration. Due to (4.3) the boundary terms vanish and one is left with the expression

$$I_a = 2^{-3} \pi^{-2} m^4 (4e^\gamma)^{4\epsilon} \frac{\Gamma(1/2 + \epsilon)^3}{\Gamma(3/2 - \epsilon)} \frac{1}{8\epsilon} \times \int_0^\infty dy y^{-8\epsilon} \frac{d}{dy} \left[B\left(y, \frac{m_1}{m}, \frac{m_2}{m}, \epsilon\right) B\left(y, \frac{m_3}{m}, \frac{m_4}{m}, \epsilon\right) B\left(y, \frac{m_5}{m}, \frac{m_6}{m}, \epsilon\right) \right], \quad (4.6)$$

where the remaining integral is completely finite. The factor $y^{-8\epsilon}$ can now be expanded in ϵ leading to

$$\begin{aligned} I_a &= 2^{-3} \pi^{-2} m^4 (4e^\gamma)^{4\epsilon} \frac{\Gamma(1/2 + \epsilon)^3}{\Gamma(3/2 - \epsilon)} \\ &\times \left(\frac{1}{8\epsilon} \int_0^\infty B\left(y, \frac{m_1}{m}, \frac{m_2}{m}, \epsilon\right) B\left(y, \frac{m_3}{m}, \frac{m_4}{m}, \epsilon\right) B\left(y, \frac{m_5}{m}, \frac{m_6}{m}, \epsilon\right) \right. \\ &\left. - \int_0^\infty dy \ln y \frac{d}{dy} \left[B\left(y, \frac{m_1}{m}, \frac{m_2}{m}, \epsilon\right) B\left(y, \frac{m_3}{m}, \frac{m_4}{m}, \epsilon\right) B\left(y, \frac{m_5}{m}, \frac{m_6}{m}, \epsilon\right) \right] \right) \\ &= 2^{-3} \pi^{-2} m^4 (4e^\gamma)^{4\epsilon} \frac{\Gamma(1/2 + \epsilon)^3}{\Gamma(3/2 - \epsilon)} \left(\frac{1}{8\epsilon} \left(\frac{2^{2\epsilon} \sqrt{\pi} \Gamma(1/2 - \epsilon)}{\Gamma(1 - \epsilon)} \right)^3 \right. \\ &\left. - 8 \int_0^\infty dy \ln y \frac{d}{dy} \left[\arctan\left(\frac{my}{m_1 + m_2}\right) \arctan\left(\frac{my}{m_3 + m_4}\right) \arctan\left(\frac{my}{m_5 + m_6}\right) \right] \right). \quad (4.7) \end{aligned}$$

Here I have used the result (4.4) and in addition suppressed $\mathcal{O}(\epsilon)$ terms.

Using the value $\psi(1) = -\gamma$ one may expand also the first term in (4.7) finally obtaining:

$$I_a = 2^{-5} \pi^2 m^4 \left(\frac{1}{\epsilon} + 12 \ln 2 + 2 - \frac{64}{\pi^3} \int_0^\infty dy \ln y \frac{d}{dy} \left[\arctan\left(\frac{my}{m_1 + m_2}\right) \arctan\left(\frac{my}{m_3 + m_4}\right) \arctan\left(\frac{my}{m_5 + m_6}\right) \right] \right). \quad (4.8)$$

It seems that the remaining integral can be performed analytically only in some special cases. One such case is when $m_1 + m_2 = m_3 + m_4 = m_5 + m_6 \equiv M$. One then has:

$$I_a = 2^{-5} \pi^2 m^4 \left(\frac{1}{\epsilon} + 12 \ln 2 + 2 - 4 \left(2 \ln \frac{M}{m} + \frac{21}{\pi^2} \zeta(3) \right) \right), \quad (4.9)$$

which in the case of identical propagator masses ($m_i = m \forall i$) gives numerically:

$$I_a(m, \dots, m) \approx 0.3084251375 \left(\frac{1}{\epsilon} - 5.4580928494 \right) \times m^4 \quad (4.10)$$

4.2 Diagram *b*

If an extra propagator with mass m_7 is added to the triangle diagram, it becomes finite in three dimensions. Using the above calculations one may then instantly write it in the form analogous to (4.5):

$$I_b = \frac{2m^2}{\pi} \int_0^\infty dy \left(\frac{1}{y \left(y^2 + \frac{m_7^2}{m^2} \right)} \arctan \left(\frac{my}{m_1 + m_2} \right) \right. \\ \left. \times \arctan \left(\frac{my}{m_3 + m_4} \right) \arctan \left(\frac{my}{m_5 + m_6} \right) \right). \quad (4.11)$$

This integral can easily be evaluated numerically with each mass configuration. When all masses are identical one obtains:

$$I_b(m, \dots, m) = 0.1291074598 \times m^2. \quad (4.12)$$

4.3 Diagram *c*

The N diagram is also clearly finite in three dimensions so one may at once set $\epsilon = 0$. Taking advantage of the familiar subdiagrams one is able to perform two momentum integrations, which eventually results in the formula

$$I_c = \frac{m^4}{4\pi^4} \int d^3p \int d^3q \frac{1}{\sqrt{p^2 q^2}} \arctan \left(\frac{|p|}{m_1 + m_2} \right) \arctan \left(\frac{|q|}{m_3 + m_4} \right) \\ \times \frac{1}{p^2 + m_5^2} \frac{1}{q^2 + m_6^2} \frac{1}{(p - q)^2 + m_7^2}. \quad (4.13)$$

The angular integrals can be calculated in a straightforward way leading to a two-dimensional integral representation for the N diagram:

$$I_c = \frac{m^2}{\pi^2} \int_0^\infty dx \int_0^\infty dy \arctan \left(\frac{mx}{m_1 + m_2} \right) \arctan \left(\frac{my}{m_3 + m_4} \right) \\ \times \frac{1}{x^2 + \frac{m_5^2}{m^2}} \frac{1}{y^2 + \frac{m_6^2}{m^2}} \ln \left(\frac{(x + y)^2 + \frac{m_7^2}{m^2}}{(x - y)^2 + \frac{m_7^2}{m^2}} \right). \quad (4.14)$$

Again it seems that the remaining integrals can only be performed numerically with the possible exception of some special mass configurations. In the case $m_i = m \forall i$ one obtains

$$I_c(m, \dots, m) = 0.1077181618 \times m^2. \quad (4.15)$$

Chapter 5

Diagrams evaluated in coordinate space

5.1 Preliminaries

When the number of vertices in a diagram is small, one possibly fruitful approach is to convert the momentum space integrations into coordinate space ones by taking Fourier transforms of the propagators. This is based on the fact that the number of coordinate space integrals needed in each case is one less than the number of vertices. The coordinate representation of a propagator is, however, considerably more complicated than the momentum one and in addition the angular integrals often prove to be very difficult in coordinate space. This method has been used extensively e.g. by Braaten and Nieto [13] and by Groote, Körner and Pivovarov [19], whose results in angular integrals I will quote in the following.

The fundamental formula in coordinate space calculations is the $3 - 2\epsilon$ -dimensional Fourier transform of a massive propagator:

$$D(x, m_a) \equiv \frac{m_a^{2\epsilon}}{(2\pi)^{3-2\epsilon}} \int d^{3-2\epsilon} p \frac{e^{-ip \cdot x}}{p^2 + m_a^2} = \frac{m_a^{2\epsilon}}{(2\pi)^{3/2-\epsilon}} \left(\frac{m_a}{x}\right)^{1/2-\epsilon} K_{1/2-\epsilon}(m_a x), \quad (5.1)$$

where $K_{1/2-\epsilon}$ denotes a modified Bessel function. When expanded with respect to x at small values of the variable the propagator gives

$$\begin{aligned} D(x, m_a) &= \frac{m_a^{2\epsilon} \Gamma(1/2 - \epsilon)}{4\pi^{1-\epsilon} \Gamma(1/2)} x^{-1+2\epsilon} \left(1 + \frac{(m_a x)^2}{2(1+2\epsilon)} + \mathcal{O}((m_a x)^4) \right) \\ &\quad - \frac{m_a^{2\epsilon} \Gamma(-1/2 + \epsilon)}{(4\pi)^{1-\epsilon} \Gamma(-1/2)} m_a^{1-2\epsilon} \left(1 + \mathcal{O}((m_a x)^2) \right) \\ &\equiv m_a^{1-2\epsilon} \left[\alpha (m_a x)^{-1+2\epsilon} \left(1 + \frac{(m_a x)^2}{2(1+2\epsilon)} + \mathcal{O}((m_a x)^4) \right) \right. \\ &\quad \left. - \beta \left(1 + \mathcal{O}((m_a x)^2) \right) \right], \end{aligned} \quad (5.2)$$

where the coefficients α and β have the following ϵ -expansions:

$$\begin{aligned}\alpha &= \frac{m^{2\epsilon}\Gamma(1/2-\epsilon)}{4\pi^{1-\epsilon}\Gamma(1/2)} = \frac{1}{4\pi} \left(1 + \epsilon \left[\gamma + \ln(4\pi m^2) \right] \right. \\ &\quad \left. + \frac{\epsilon^2}{4} \left[\pi^2 + 2\gamma^2 + 4\gamma \ln(4\pi m^2) + 2(4\pi m^2)^2 \right] + \mathcal{O}(\epsilon^3) \right), \\ \beta &= \frac{m^{2\epsilon}\Gamma(-1/2+\epsilon)}{(4\pi)^{1-\epsilon}\Gamma(-1/2)} = \frac{1}{4\pi} \left(1 + \epsilon \left[2 - \gamma + \ln(\pi m^2) \right] + \mathcal{O}(\epsilon^2) \right).\end{aligned}\quad (5.3)$$

Correspondingly, the ϵ -expansion of D itself is

$$D(x, m_a) = \frac{e^{-m_a x}}{4\pi x} \left(1 + \epsilon \left(\ln\left(\frac{2\pi m^2 x}{m_a}\right) + e^{2m_a x} \text{Ei}(-2m_a x) \right) + \mathcal{O}(\epsilon^2) \right), \quad (5.4)$$

where $\text{Ei}(x)$ denotes the exponential integral and the relations (equations 8.469 and 8.486(1) of [38])

$$K_{1/2}(x) = \sqrt{\frac{\pi}{2x}} e^{-x} \quad (5.5)$$

$$\left[\frac{\partial K_\nu(x)}{\partial \nu} \right]_{\nu=1/2} = - \left(\frac{\pi}{2x} \right)^{1/2} e^x \text{Ei}(-2x) \quad (5.6)$$

have been used.

5.2 Diagram d

The basketball-type diagrams containing only two vertices are especially well suited for integration in coordinate space due to their trivial angular structure there. After writing the propagators in terms of their Fourier transforms one obtains in the four-loop case:

$$\begin{aligned}I_d &= m^{-10\epsilon} \left(\frac{4\pi m^{1+2\epsilon}}{(\pi e^{-\gamma})^\epsilon} \right)^4 \int d^{3-2\epsilon} x \prod_{i=1}^5 D(x, m_i) \\ &= \left(\frac{4\pi m^{1-\epsilon/2}}{(\pi e^{-\gamma})^\epsilon} \right)^4 \frac{2\pi^{3/2-\epsilon}}{\Gamma(3/2-\epsilon)} \int_0^\infty dx x^{2-2\epsilon} \prod_{i=1}^5 D(x, m_i) \\ &\equiv \left(\frac{4\pi m^{1-\epsilon/2}}{(\pi e^{-\gamma})^\epsilon} \right)^4 \frac{2\pi^{3/2-\epsilon}}{\Gamma(3/2-\epsilon)} \mathcal{I}.\end{aligned}\quad (5.7)$$

It can be easily seen that the integral \mathcal{I} diverges near the origin. One may then simplify the calculation by introducing a small parameter r and dividing the radial integration line into two subintervals $[0, r]$ and $[r, \infty[$ ($\mathcal{I} \equiv \mathcal{I}_1 + \mathcal{I}_2$). On the first interval the small- x expansion of the propagators can be used, whereas on the latter one may simply set $\epsilon = 0$. The parameter r is considered to be arbitrarily small but nonzero so that all contributions to the integrals

proportional to its positive powers can immediately be neglected. If the calculations are performed correctly, all r -dependence will in any case naturally vanish from the final result.

Using (5.2) one obtains on the first interval:

$$\mathcal{I}_1 = \int_0^r dx x^{2-2\epsilon} \times \prod_{i=1}^5 \left(m_i^{1-2\epsilon} \left[\alpha (m_i x)^{-1+2\epsilon} \left(1 + \frac{(m_i x)^2}{2(1+2\epsilon)} + \mathcal{O}((m_i x)^4) \right) - \beta \left(1 + \mathcal{O}((m_i x)^2) \right) \right] \right), \quad (5.8)$$

which reads after neglecting the terms that vanish in the limit $r \rightarrow 0$:

$$\mathcal{I}_1 = \int_0^r dx x^{2-2\epsilon} \left(\alpha^5 x^{-5+10\epsilon} - \alpha^4 \beta \sum_{i=1}^5 m_i^{1-2\epsilon} x^{-4+8\epsilon} + \frac{\alpha^5}{2(1+2\epsilon)} \sum_{i=1}^5 m_i^2 x^{-3+10\epsilon} + \frac{\alpha^3 \beta^2}{2} \sum_{i \neq j} (m_i m_j)^{1-2\epsilon} x^{-3+6\epsilon} \right). \quad (5.9)$$

If ϵ is assumed to be large enough for the lower limits to vanish (later one may analytically continue the result to the neighborhood of $\epsilon = 0$) and irrelevant (higher order in ϵ) terms are dropped, the integrations can be straightforwardly performed with the result:

$$\mathcal{I}_1 = -\frac{\alpha^5}{2} r^{-2} + \alpha^4 \beta \overbrace{\sum_{i=1}^5 m_i}^M r^{-1} + \frac{\alpha^5 r^{8\epsilon}}{16\epsilon(1+2\epsilon)} \sum_{i=1}^5 m_i^2 + \frac{\alpha^3 \beta^2 r^{4\epsilon}}{8\epsilon} \sum_{i \neq j} (m_i m_j)^{1-2\epsilon} \quad (5.10)$$

On the second interval the calculation is considerably easier, since with $\epsilon = 0$ one only needs to evaluate the integral

$$\mathcal{I}_2 = \frac{1}{(4\pi)^5} \int_r^\infty dx \frac{e^{-Mx}}{x^3}. \quad (5.11)$$

Performing several partial integrations and at each step dropping terms that vanish when $r \rightarrow 0$ one eventually obtains:

$$\begin{aligned} \mathcal{I}_2 &= \frac{1}{(4\pi)^5} \left(\frac{e^{-Mr}}{2r^2} - \frac{M e^{-Mr}}{2r} - \frac{M^2 e^{-Mr} \ln(Mr)}{2} + \frac{M^2}{2} \int_0^\infty dx \ln x e^{-x} \right) \\ &= \frac{1}{(4\pi)^5} \left(\frac{1}{2r^2} - \frac{M}{r} + \frac{1}{2} \left(\frac{3}{2} - \gamma \right) M^2 - \frac{M^2 \ln(Mr)}{2} \right). \end{aligned} \quad (5.12)$$

Adding up \mathcal{I}_1 and \mathcal{I}_2 , expanding to 0th order in ϵ and simplifying the result in a straightforward manner one may now write down the result for the whole diagram:

$$\begin{aligned} I_d &= m^4 \left(\left(1 + \epsilon \left[2 + 3\gamma - \ln(4\pi^5 m^2) \right] \right) \right. \\ &\quad \times \left. \left(\frac{1}{16\epsilon} \left[\sum_{i=1}^5 m_i^2 + 2 \sum_{i \neq j} m_i m_j \right] + \frac{1}{16} \left(-2 + 5\gamma + 5 \ln(4\pi m^2) \right) \sum_{i=1}^5 m_i^2 + \right. \right. \end{aligned}$$

$$\begin{aligned}
& \frac{1}{8} \left(4 + \gamma + \ln \left(2^6 \pi^5 m^{10} \right) \right) \sum_{i \neq j} m_i m_j - \frac{1}{2} \sum_{i \neq j} m_i m_j \ln m_i \\
& + \frac{M^2}{2} \left(\frac{3}{2} - \gamma \right) - \frac{M^2 \ln M}{2} \\
& = \frac{M^2 m^4}{2} \left(\frac{1}{8\epsilon} \left[1 + \sum_{i \neq j} \frac{m_i m_j}{M^2} \right] + \frac{3}{2} + \ln \left(\frac{2m}{M} \right) + \sum_{i \neq j} \frac{m_i m_j}{M^2} \left(\ln \left(\frac{m}{m_i} \right) + \frac{3}{2} \right) \right).
\end{aligned} \tag{5.13}$$

When all masses are equal one obtains:

$$I_d(m, \dots, m) = \frac{45m^6}{16} \left(\frac{1}{\epsilon} + 12 + \frac{40}{9} \ln \frac{2}{5} \right) \approx 2.8125 \left(\frac{1}{\epsilon} + 7.9275967472 \right) \times m^6 \tag{5.14}$$

5.3 Diagram *e*

This divergent diagram has a rather complicated structure and its analytic evaluation in momentum space might well turn out to be impossible. First Fourier-transforming the propagators and then performing the momentum integrals with help of delta-functions one, however, ends up with the more manageable formula:

$$\begin{aligned}
I_e &= \left(\frac{4\pi m^{1-\epsilon}}{(\pi e^{-\gamma})^\epsilon} \right)^4 \int d^{3-2\epsilon} x \int d^{3-2\epsilon} y \, D(|x-y|, m_1) \\
&\quad \times D(x, m_2) D(x, m_3) D(y, m_4) D(y, m_5) D(y, m_6),
\end{aligned} \tag{5.15}$$

which is illustrated by the picture



$$\tag{5.16}$$

The angular integrations of (5.15) can be performed using the identity

$$\int d\Omega_\rho \frac{K_\lambda(|r-\rho|)}{|r-\rho|^\lambda} = (2\pi)^{\lambda+1} \frac{I_\lambda(\rho)}{\rho^\lambda} \frac{K_\lambda(r)}{r^\lambda} \tag{5.17}$$

derived by Groote et al. [19] and which holds when $r > \rho$. This leads to the expression:

$$\begin{aligned}
I_e &= \left(\frac{4\pi m}{(\pi e^{-\gamma})^\epsilon} \right)^4 \int_0^\infty dx \int_0^\infty dy \, x^{2-2\epsilon} y^{2-2\epsilon} \prod_{i=2}^3 D(x, m_i) \prod_{i=4}^6 D(y, m_i) \\
&\quad \times (D(x, m_1) G(m_1 y) \theta(x-y) + D(y, m_1) G(m_1 x) \theta(y-x)) \\
&\equiv \left(\frac{4\pi m}{(\pi e^{-\gamma})^\epsilon} \right)^4 \mathcal{I},
\end{aligned} \tag{5.18}$$

where

$$G(m_a x) = \frac{2^{5/2-\epsilon} \pi^{3-2\epsilon}}{\Gamma(3/2-\epsilon) m^{4\epsilon}} \frac{I_{1/2-\epsilon}(m_a x)}{(m_a x)^{1/2-\epsilon}}. \tag{5.19}$$

The function G has the small- x -expansion

$$\begin{aligned} G(m_a x) &= \frac{4\pi^{3-2\epsilon}}{\Gamma(3/2 - \epsilon)^2 m^{4\epsilon}} \left(1 + \mathcal{O}\left((m_a x)^2\right)\right) \\ &\equiv \kappa \left(1 + \mathcal{O}\left((m_a x)^2\right)\right), \end{aligned} \quad (5.20)$$

where the coefficient κ further has the ϵ -expansion

$$\begin{aligned} \kappa &= \frac{4\pi^{3-2\epsilon}}{\Gamma(3/2 - \epsilon)^2 m^{4\epsilon}} = (4\pi)^2 \left(1 + 2\epsilon \left[2 - \gamma - \ln(4\pi m^2)\right] \right. \\ &\quad \left. + \epsilon^2 \left[12 - \frac{\pi^2}{2} - 8\gamma + 2\gamma^2 + 4(\gamma - 2) \ln(4\pi m^2) + 2(4\pi m^2)^2\right] + \mathcal{O}(\epsilon^3)\right). \end{aligned} \quad (5.21)$$

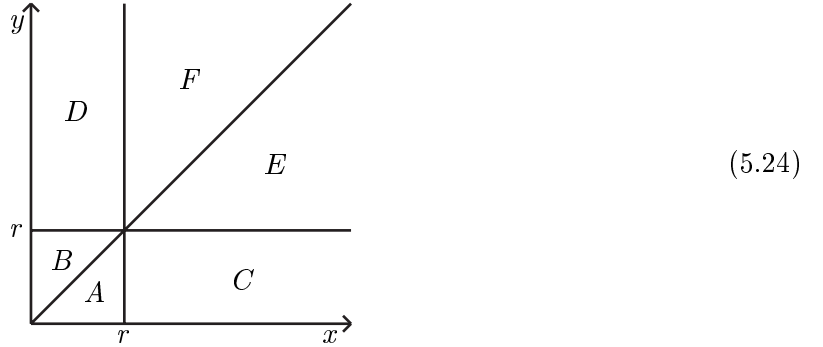
With ϵ set to zero G reads

$$G(m_a x) = (4\pi)^2 \frac{\sinh(m_a x)}{m_a x}. \quad (5.22)$$

Since it is obvious that the divergence of \mathcal{I} comes from the UV area, one may again simplify the calculation by dividing the integration plane into different regions:

$$\begin{aligned} \text{A} &: 0 \leq y \leq x \leq r \\ \text{B} &: 0 \leq x \leq y \leq r \\ \text{C} &: 0 \leq y \leq r \leq x < \infty \\ \text{D} &: 0 \leq x \leq r \leq y < \infty \\ \text{E} &: r \leq y \leq x < \infty \\ \text{F} &: r \leq x \leq y < \infty, \end{aligned} \quad (5.23)$$

which is depicted in the diagram below. The parameter r can as before be thought to be arbitrarily small but nonzero, and hence I will at each stage of the calculations discard terms that vanish as $r \rightarrow 0$.



From now on I will use a new notation for the sums and products of masses:

$$\begin{aligned} m_i + m_j + m_k + \dots &\equiv M_{ijk\dots} \\ m^i \times m^j \times m^k \times \dots &\equiv M^{ijk\dots}. \end{aligned} \quad (5.25)$$

Region A

In this integration region the variables x and y are arbitrarily small so one may certainly use the small- x expansions. Denoting $y = tx$ (Jacobian = x) and neglecting terms that vanish in the limit $r \rightarrow 0$ one obtains

$$\begin{aligned}
\mathcal{I}_A &= \int_0^r dx \int_0^x dy x^{2-2\epsilon} y^{2-2\epsilon} G(m_1 y) \prod_{i=1}^3 D(x, m_i) \prod_{i=4}^6 D(y, m_i) \\
&= \kappa \alpha^6 \int_0^r dx \int_0^1 dt x^{-1+8\epsilon} t^{-1+4\epsilon} = \kappa \alpha^6 \frac{r^{8\epsilon}}{32\epsilon^2} \\
&= \frac{1}{32(4\pi)^4} \left(\frac{1}{\epsilon^2} + \frac{4}{\epsilon} \left[1 + \gamma + \ln(4\pi m^2 r^2) \right] \right. \\
&\quad \left. + 4 \left[3 + \frac{\pi^2}{4} + 4\gamma + 2\gamma^2 + 4(1 + \gamma) \ln(4\pi m^2 r^2) + 2 \left(\ln(4\pi m^2 r^2) \right)^2 \right] \right). \quad (5.26)
\end{aligned}$$

Region B

In region B the calculation proceeds exactly in the same fashion as in the previous one and one is straightforwardly lead to the expression

$$\begin{aligned}
\mathcal{I}_B &= \int_0^r dy \int_0^y dx x^{2-2\epsilon} y^{2-2\epsilon} G(m_1 x) D(y, m_1) \prod_{i=2}^3 D(x, m_i) \prod_{i=4}^6 D(y, m_i) \\
&= \kappa \alpha^6 \frac{r^{8\epsilon}}{8\epsilon(1+2\epsilon)} = \frac{1}{8(4\pi)^4} \left(\frac{1}{\epsilon} + 2 \left[1 + 2\gamma + 2 \ln(4\pi m^2 r^2) \right] \right). \quad (5.27)
\end{aligned}$$

Region C

In the evaluation of the diagram e it is the region C that clearly produces the most difficulties. This is due to the fact that while the y -integral contains here a divergent contribution from the region near the origin necessitating the use of a nonzero ϵ , the x -integration is being performed from r to ∞ making the application of the small- x -expansion for $D(x, m_i)$ impossible. Proceeding as before one obtains:

$$\begin{aligned}
\mathcal{I}_C &= \int_r^\infty dx \int_0^r dy x^{2-2\epsilon} y^{2-2\epsilon} G(m_1 y) \prod_{i=1}^3 D(x, m_i) \prod_{i=4}^6 D(y, m_i) \\
&= \kappa \alpha^3 \int_r^\infty dx x^{2-2\epsilon} \prod_{i=1}^3 D(x, m_i) \int_0^r dy y^{-1+4\epsilon} \\
&= \kappa \alpha^3 \frac{r^{4\epsilon}}{4\epsilon} \int_r^\infty dx x^{2-2\epsilon} \prod_{i=1}^3 D(x, m_i). \quad (5.28)
\end{aligned}$$

In order to obtain also the finite part of \mathcal{I}_C one must now apply the ϵ -expansion of D (5.4) in the x-integral resulting in

$$\begin{aligned} & \int_r^\infty dx x^{2-2\epsilon} \prod_{i=1}^3 D(x, m_i) \\ &= \frac{1}{(4\pi)^3} \int_r^\infty dx \frac{e^{-M_{123}x}}{x} \left[1 + \epsilon \left(\ln x + 3 \ln(2\pi m^2) - \ln M^{123} + \sum_{i=1}^3 e^{2m_i x} \text{Ei}(-2m_i x) \right) \right]. \end{aligned} \quad (5.29)$$

The evaluation of this integral requires the calculation of several elementary one-dimensional integrals on the interval $[r, \infty[$. Performing partial integrations, using standard formulae and neglecting terms that vanish in the limit $r \rightarrow 0$ one obtains:

$$\begin{aligned} \int_r^\infty dx \frac{e^{-kx}}{x} &\equiv -\text{Ei}(-kr) \\ &= \left|_{kr}^\infty \ln x e^{-x} + \int_0^\infty dx \ln x e^{-x} - \int_0^{kr} dx \ln x e^{-x} \right. \\ &= -\ln(kr) e^{-kr} - \gamma \\ &= -\gamma - \ln(kr) \end{aligned} \quad (5.30)$$

$$\begin{aligned} \int_r^\infty dx \frac{e^{-kx}}{x} \ln x &= \int_{kr}^\infty dx \frac{e^{-x}}{x} (\ln x - \ln k) \\ &= \frac{1}{2} \left|_{kr}^\infty (\ln x)^2 e^{-x} + \frac{1}{2} \int_0^\infty (\ln x)^2 e^{-x} - \ln k \int_{kr}^\infty dx \frac{e^{-x}}{x} \right. \\ &= \ln k (\gamma + \ln(kr)) - \frac{1}{2} (\ln(kr))^2 + \frac{1}{2} \left(\frac{\pi^2}{6} + \gamma^2 \right) \\ &\equiv f(k, r) \end{aligned} \quad (5.31)$$

$$\begin{aligned} \int_r^\infty dx \frac{e^{-kx}}{x} \text{Ei}(-2mx) &= \left|_{kr}^\infty \ln x e^{-x} \text{Ei}\left(-\frac{2m}{k}x\right) - \int_{kr}^\infty dx \ln x \frac{e^{-(1+\frac{2m}{k})x}}{x} \right. \\ &\quad \left. + \int_0^\infty dx \ln x e^{-x} \text{Ei}\left(-\frac{2m}{k}x\right) \right. \\ &= -\ln(kr) e^{-kr} \text{Ei}(-2mr) - f\left(\frac{2m}{k} + 1, kr\right) - \text{Li}_2\left(-\frac{k}{2m}\right) \\ &\quad \left. + \frac{1}{2} \ln\left(1 + \frac{k}{2m}\right) \left(2\gamma + \ln\left(\frac{2m}{k} \left(1 + \frac{2m}{k}\right)\right) \right) \right. \\ &= -\frac{1}{2} \left(\frac{\pi^2}{6} + \gamma^2 \right) - \text{Li}_2\left(-\frac{k}{2m}\right) - \gamma \ln(2mr) - \frac{1}{2} (\ln(2mr))^2. \end{aligned} \quad (5.32)$$

In the final stage of the last integral the results of the two previous ones have been used.

Returning to (5.29) one may now write

$$\int_r^\infty dx x^{2-2\epsilon} \prod_{i=1}^3 D(x, m_i)$$

$$\begin{aligned}
&= \frac{1}{(4\pi)^3} \left(-\gamma - \ln(M_{123}r) \right. \\
&+ \epsilon \left[\left(3 \ln(2\pi m^2) - \ln M^{123} \right) \left(-\gamma - \ln(M_{123}r) \right) + f(M_{123}, r) \right. \\
&+ \left. \left. \sum_{i=1}^3 \left(-\frac{1}{2} \left(\frac{\pi^2}{6} + \gamma^2 \right) - \text{Li}_2 \left(-\frac{M_{123} - 2m_i}{2m_i} \right) - \gamma \ln(2m_i r) - \frac{1}{2} (\ln(2m_i r))^2 \right) \right] \right) \\
&= \frac{1}{(4\pi)^3} \left(-\left(\gamma + \ln(M_{123}r) \right) \left(1 + \epsilon \left[3 \ln(2\pi m^2) - \ln(M_{123}M^{123}) \right] \right) \right. \\
&+ \epsilon \left[-\frac{\pi^2}{6} - \gamma^2 - \frac{1}{2} (\ln(M_{123}r))^2 \right. \\
&- \left. \left. \sum_{i=1}^3 \left(\frac{1}{2} (\ln(2m_i r))^2 + \gamma \ln(2m_i r) + \text{Li}_2 \left(1 - \frac{M_{123}}{2m_i} \right) \right) \right] \right). \tag{5.33}
\end{aligned}$$

Using this result in (5.28) and simplifying the result the contribution of region C to \mathcal{I} is now finally available:

$$\begin{aligned}
\mathcal{I}_C &= -\frac{1}{4(4\pi)^4} \left(\left(\gamma + \ln(M_{123}r) \right) \left(\frac{1}{\epsilon} + 4 + \gamma + \ln 2 + 4 \ln(2\pi m^2 r) - \ln(M_{123}M^{123}) \right) \right. \\
&+ \frac{\pi^2}{6} + \gamma^2 + \frac{1}{2} (\ln(M_{123}r))^2 \\
&+ \left. \sum_{i=1}^3 \left(\frac{1}{2} (\ln(2m_i r))^2 + \gamma \ln(2m_i r) + \text{Li}_2 \left(1 - \frac{M_{123}}{2m_i} \right) \right) \right). \tag{5.34}
\end{aligned}$$

Region D

This region produces no divergences so one may set $\epsilon = 0$ in the beginning. Then the integrals reduce to familiar types and going once again to the limit $r \rightarrow 0$ one obtains

$$\begin{aligned}
\mathcal{I}_D &= \int_0^r dx \int_r^\infty dy x^2 y^2 G(m_1 x) D(y, m_1) \prod_{i=2}^3 D(x, m_i) \prod_{i=4}^6 D(y, m_i) \\
&= \frac{1}{(4\pi)^4 m_1} \int_0^r dx \frac{e^{-M_{23}x}}{x} \sinh(m_1 x) \int_r^\infty dy \frac{e^{-M_{1456}y}}{y^2} \\
&= \frac{1}{(4\pi)^4 m_1} m_1 r \left(\frac{e^{-M_{1456}r}}{r} + M_{1456} \text{Ei}(-M_{1456}r) \right) \\
&= \frac{M_{1456}r}{(4\pi)^4} \left(\frac{1}{M_{1456}r} - 1 + \gamma + \ln(M_{1456}r) \right) = \frac{1}{(4\pi)^4}. \tag{5.35}
\end{aligned}$$

Region E

Since the region E contains no points near the origin, one easily observes that its contribution to the integral \mathcal{I} is also finite. Proceeding as before one may write

$$\begin{aligned}
\mathcal{I}_E &= \int_r^\infty dy \int_y^\infty dx x^2 y^2 G(m_1 y) \prod_{i=1}^3 D(x, m_i) \prod_{i=4}^6 D(y, m_i) \\
&= \frac{1}{(4\pi)^4 m_1} \int_r^\infty dy \frac{e^{-M_{456} y}}{y^2} \sinh(m_1 y) \int_y^\infty dx \frac{e^{-M_{123} x}}{x} \\
&= -\frac{1}{(4\pi)^4 m_1} \int_r^\infty dy \frac{e^{-M_{456} y}}{y^2} \sinh(m_1 y) \text{Ei}(-M_{123} y) \\
&= \frac{M_{123}}{2(4\pi)^4 m_1} \int_{M_{123} r}^\infty dy y^{-2} \text{Ei}(-y) \left(e^{-\frac{M_{1456}}{M_{123}} y} - e^{-\frac{-m_1 + M_{456}}{M_{123}} y} \right).
\end{aligned} \tag{5.36}$$

It is obvious that one now has to evaluate an integral of the form $\int_r^\infty dy y^{-2} \text{Ei}(-y) e^{-ky}$. In the limit $r \rightarrow 0$ one obtains

$$\begin{aligned}
\int_r^\infty dy \frac{e^{-ky}}{y^2} \text{Ei}(-y) &= -\left|_r^\infty \frac{e^{-ky}}{y} \text{Ei}(-y) - k \int_r^\infty dy \frac{e^{-ky}}{y} \text{Ei}(-y) + \int_r^\infty dy \frac{e^{-(k+1)y}}{y^2} \right. \\
&= \frac{e^{-kr}}{r} \text{Ei}(-r) - k \left|_r^\infty \ln y e^{-ky} \text{Ei}(-y) - k^2 \int_0^\infty dy \ln y e^{-ky} \text{Ei}(-y) \right. \\
&\quad + k \int_r^\infty dy \frac{e^{-(k+1)y}}{y} \ln y - \left|_r^\infty \frac{e^{-(k+1)y}}{y} - (k+1) \int_r^\infty dy \frac{e^{-(k+1)y}}{y} \right. \\
&= \frac{e^{-kr}}{r} \text{Ei}(-r) + k \ln r e^{-kr} \text{Ei}(-r) \\
&\quad - k \left(\gamma \ln(k+1) + \frac{1}{2} (\ln(1+k))^2 - \text{Li}_2(-k) \right) \\
&\quad + k f(k+1, r) + \frac{e^{-(k+1)r}}{r} + (k+1) \text{Ei}(-(k+1)r) \\
&= \frac{\ln r}{r} + \frac{1+\gamma}{r} + \frac{k}{2} (\ln r)^2 + (1+\gamma k) \ln r - k - 1 + \gamma + \\
&\quad (k+1) \ln(k+1) + k \text{Li}_2(-k) + \frac{k}{2} \left(\frac{\pi^2}{6} + \gamma^2 \right) \\
&= \frac{\ln r}{r} + \frac{1+\gamma}{r} + \ln r - 1 + \gamma + k \left(\frac{(\ln r)^2}{2} + \gamma \ln r - 1 + \right. \\
&\quad \left. \text{Li}_2(-k) + \frac{1}{2} \left(\frac{\pi^2}{6} + \gamma^2 \right) \right) + (k+1) \ln(k+1).
\end{aligned} \tag{5.37}$$

Using (5.37) \mathcal{I}_E can be straightforwardly written down:

$$\mathcal{I}_E = \frac{1}{2(4\pi)^4} \left(-2 + \frac{\pi^2}{6} + \gamma^2 + \frac{M_{1123456}}{m_1} \ln \left(\frac{M_{1123456}}{M_{123}} \right) - \frac{M_{23456}}{m_1} \ln \left(\frac{M_{23456}}{M_{123}} \right) \right)$$

$$\begin{aligned}
& + \frac{M_{1456}}{m_1} \operatorname{Li}_2 \left(-\frac{M_{1456}}{M_{123}} \right) + \left(1 - \frac{M_{456}}{m_1} \right) \operatorname{Li}_2 \left(-\frac{-m_1 + M_{456}}{M_{123}} \right) \\
& + 2\gamma \ln(M_{123}r) + (\ln(M_{123}r))^2 \Big). \tag{5.38}
\end{aligned}$$

Region F

The calculation in region F follows very closely that of the preceding section. Setting $\epsilon = 0$ one gets

$$\begin{aligned}
\mathcal{I}_F &= \int_r^\infty dx \int_x^\infty dy x^2 y^2 G(m_1 x) D(y, m_1) \prod_{i=2}^3 D(x, m_i) \prod_{i=4}^6 D(y, m_i) \\
&= \frac{1}{(4\pi)^4 m_1} \int_r^\infty dx \frac{e^{-M_{23}x}}{x} \sinh(m_1 x) \int_x^\infty dy \frac{e^{-M_{1456}y}}{y^2} \\
&= \frac{1}{(4\pi)^4 m_1} \int_r^\infty dx \frac{e^{-M_{23}x}}{x} \sinh(m_1 x) \left(\frac{e^{-M_{1456}x}}{x} + M_{1456} \operatorname{Ei}(-M_{1456}x) \right) \\
&= \frac{1}{(4\pi)^4 m_1} \left(\frac{1}{2r} \left(e^{-M_{23456}r} - e^{-M_{1123456}r} \right) \right. \\
&\quad + \frac{M_{23456}}{2} \operatorname{Ei}(-M_{23456}r) - \frac{M_{1123456}}{2} \operatorname{Ei}(-M_{1123456}r) \\
&\quad \left. + \frac{M_{1456}}{2} \int_r^\infty dx x^{-1} \operatorname{Ei}(-M_{1456}x) \left(e^{-(-m_1+M_{23})x} - e^{-M_{123}x} \right) \right). \tag{5.39}
\end{aligned}$$

Going once again to the limit $r \rightarrow 0$ and using a previous result (5.32) one obtains

$$\begin{aligned}
\mathcal{I}_F &= \frac{1}{2(4\pi)^4} \left(2(1-\gamma) + \frac{M_{23456}}{m_1} \ln(M_{23456}r) - \frac{M_{1123456}}{m_1} \ln(M_{1123456}r) \right. \\
&\quad \left. + \frac{M_{1456}}{m_1} \left(\operatorname{Li}_2 \left(-\frac{M_{123}}{M_{1456}} \right) - \operatorname{Li}_2 \left(-\frac{-m_1 + M_{23}}{M_{1456}} \right) \right) \right). \tag{5.40}
\end{aligned}$$

Final result

Adding up the contributions from the different regions one may now finally write down the result for the whole diagram. After some straightforward simplifications it reads

$$\begin{aligned}
I_e &= \frac{m^4}{32} \left(\frac{1}{\epsilon^2} + \frac{8}{\epsilon} \left[1 + \ln \left(\frac{2m}{M_{123}} \right) \right] \right. \\
&\quad + 4 \left[13 + \frac{7\pi^2}{12} - 3(\ln 2)^2 + 16 \ln \left(\frac{2m}{M_{123}} \right) + 8 \left(\ln \left(\frac{2m}{M_{123}} \right) \right)^2 \right. \\
&\quad \left. \left. + 2 \ln 2 \ln \left(\frac{(M_{123})^3}{M^{123}} \right) + \ln M_{123} \ln \left(\frac{(M^{123})^2}{(M_{123})^3} \right) \right] \right)
\end{aligned}$$

$$\begin{aligned}
& +4 \frac{M_{1456}}{m_1} \text{Li}_2 \left(-\frac{M_{1456}}{M_{123}} \right) + 4 \left(1 - \frac{M_{456}}{m_1} \right) \text{Li}_2 \left(-\frac{-m_1 + M_{456}}{M_{123}} \right) \\
& +4 \frac{M_{1456}}{m_1} \left(\text{Li}_2 \left(-\frac{M_{123}}{M_{1456}} \right) - \text{Li}_2 \left(-\frac{-m_1 + M_{23}}{M_{1456}} \right) \right) \\
& - \sum_{i=1}^3 \left((\ln m_i)^2 + 2 \text{Li}_2 \left(1 - \frac{M_{123}}{2m_i} \right) \right) \Bigg]. \tag{5.41}
\end{aligned}$$

All r-dependence has cancelled just as it should have so one may feel quite confident about the correctness of the result. It is interesting to note that the divergent term only depends on the first three masses through the combination $M_{123} = m_1 + m_2 + m_3$. The reason for its independence of the three other masses becomes obvious when the diagram is written in the form of an integral in momentum space and could have been anticipated already previously on the basis of the structure of the diagram in coordinate space (5.16).

Special mass configurations

An important result needed in applications of the effective QCD is obtained when the propagator masses have the values $m_3 = 0$, $m_1 = m_2 = m_4 = m_5 = m_6 = m$. Using the representation of the dilogarithm function

$$\text{Li}_2(-x) = -\frac{\pi^2}{6} - \frac{1}{2} (\ln(1+x))^2 + \int_x^\infty dt \frac{\ln(1+t)}{t(1+t)} \tag{5.42}$$

and the relation

$$\text{Li}_2(-x) + \text{Li}_2\left(-\frac{1}{x}\right) = -\frac{1}{2} (\ln(-x))^2 - \frac{\pi^2}{6} \tag{5.43}$$

one has:

$$\begin{aligned}
I_e(m, m, 0, m, m, m) &= \frac{m^4}{32} \left(\frac{1}{\epsilon^2} + \frac{8}{\epsilon} + 4 \left[13 + \frac{7\pi^2}{12} + 3(\ln 2)^2 + 2 \ln 2 \ln \left(\frac{m}{m_3} \right) \right. \right. \\
&+ \ln(2m) \ln \left(\frac{mm_3^2}{8} \right) + 16 \text{Li}_2(-2) - 8 \text{Li}_2(-1) \\
&+ 16 \left(\text{Li}_2 \left(-\frac{1}{2} \right) - \text{Li}_2(0) \right) - 2(\ln m)^2 - (\ln m_3)^2 \\
&\left. \left. - 4 \text{Li}_2(0) + 2 \left(\frac{\pi^2}{6} + \frac{1}{2} \left(\ln \left(\frac{m}{m_3} \right) \right)^2 \right) \right] \right) \\
&= \frac{m^4}{32} \left(\frac{1}{\epsilon^2} + \frac{8}{\epsilon} + 4 \left[13 - \frac{13\pi^2}{12} - 8(\ln 2)^2 \right] \right). \tag{5.44}
\end{aligned}$$

With identical masses the result is correspondingly:

$$I_e(m, \dots, m) = \frac{m^4}{32} \left(\frac{1}{\epsilon} + \frac{8}{\epsilon} \left[1 + \ln \frac{2}{3} \right] \right)$$

$$\begin{aligned}
& +4 \left[13 + \frac{7\pi^2}{12} + 5 \left(\ln \frac{2}{3} \right)^2 + 16 \ln \frac{2}{3} + 16 \left(\text{Li}_2 \left(-\frac{3}{4} \right) + \text{Li}_2 \left(-\frac{4}{3} \right) \right) \right. \\
& \left. - 8 \text{Li}_2 \left(-\frac{2}{3} \right) - 6 \text{Li}_2 \left(-\frac{1}{2} \right) - 16 \text{Li}_2 \left(-\frac{1}{4} \right) \right] \\
\approx & 0.03125 \left(\frac{1}{\epsilon^2} + 4.7562791351 \frac{1}{\epsilon} - 11.1450820899 \right) \times m^4 \quad (5.45)
\end{aligned}$$

Chapter 6

The remaining diagrams

There exists a class of four-loop scalar vacuum skeletons (the diagrams $f - j$ of figure 3.1) with such complicated topologies that neither a straightforward momentum space calculation nor a Fourier transformation and coordinate space evaluation is enough to solve them. They do not contain any simple subdiagrams and the number of vertices is too high for a successful coordinate space integration - at least using the standard formulae of Gradshteyn and Ryzhik [38] and other such tables. There remain, however, a few calculational methods to consider. Restricting oneself to previously chosen values of the propagator masses (in this chapter I will only consider the case $m_i = m \forall i$) one may perform numerical integrations exploiting the fact that all the diagrams in this class are UV-finite. Another possibility is to resort to the method of partial integration used successfully by Rajantie in [20] and derive partial differential equations that the diagrams must satisfy. Here the resulting equations will, however, be much harder to solve than the ones of [20], since the diagrams considered in this thesis do not exhibit such beautiful symmetries as the famous Mercedes diagram. I will therefore restrict myself to merely constructing the equations and will not address the question of actually solving them.

6.1 Numerical calculations

In this section I will evaluate the diagrams $f - j$ numerically assuming the masses of the different propagators to equal the m appearing in the $\overline{\text{MS}}$ measure (3.1). This procedure may seem very restrictive but it is useful to note that the methods used below can easily be generalized to any previously chosen mass configuration. The actual integrations will be performed using Mathematica and a very limited amount of CPU-time. It is therefore certainly possible to improve the accuracy of the results obtained here.

Diagram f

The structure of this diagram is clearly very complicated, since it contains as a subdiagram the 'fish' two-point function, for which no analytic expression has been found. The fish part has been considered e.g. by Rajantie in [20], where he was able to construct an one-dimensional integral representation for it in exactly three dimensions. Due to the f diagram

being UV-finite one may also here set $\epsilon = 0$ enabling the use the result, which for identical propagator masses reads:

$$\begin{aligned} \text{Diagram } f &= \frac{m}{p^2 \sqrt{p^2 + 3m^2}} \int_0^m dx \frac{1}{\sqrt{p^2 + 4m^2 - x^2}} \\ &\times \left[\frac{2p}{2m+x} \left(\arctan \left(\frac{p}{2m+x} \right) - \arctan \left(\frac{p}{2m} \right) \right) + \ln \left(\frac{p^2 + (2m+x)^2}{(2m+x)^2} \right) \right]. \end{aligned} \quad (6.1)$$

Using the above relation together with (4.2) and performing a trivial angular integration one now obtains

$$\begin{aligned} I_f(m, \dots, m) &= \frac{2}{\pi} \int_0^\infty dy \int_0^1 dt \frac{\arctan \left(\frac{y}{2} \right)}{y(1+y^2) \sqrt{y^2 + 3} \sqrt{y^2 - t^2 + 4}} \\ &\times \left[\frac{2y}{2+t} \left(\arctan \left(\frac{y}{2+t} \right) - \arctan \left(\frac{y}{2} \right) \right) + \ln \left(\frac{y^2 + (2+t)^2}{(2+t)^2} \right) \right]. \end{aligned} \quad (6.2)$$

This can be easily calculated numerically and leads to

$$I_f(m, \dots, m) \approx 0.007861658675. \quad (6.3)$$

Diagram g

With identical masses on the propagator lines the evaluation of this diagram proceeds in exact analogy with the previous one resulting in

$$\begin{aligned} I_g(m, \dots, m) &= \frac{2m^2}{\pi} \int_0^\infty dy \int_0^1 dt \frac{\arctan \left(\frac{y}{2} \right)}{y \sqrt{y^2 + 3} \sqrt{y^2 - t^2 + 4}} \\ &\times \left[\frac{2y}{2+t} \left(\arctan \left(\frac{y}{2+t} \right) - \arctan \left(\frac{y}{2} \right) \right) + \ln \left(\frac{y^2 + (2+t)^2}{(2+t)^2} \right) \right] \\ &\approx 0.07753725612 \times m^2. \end{aligned} \quad (6.4)$$

Diagram h

Denoting

$$\int d^3s \frac{1}{s^2 + m^2} \frac{1}{(s-p)^2 + m^2} \frac{1}{(s-q)^2 + m^2} \equiv g(|p|, |q|, \theta_{p,q}) \quad (6.5)$$

one easily sees that the wheel diagram may be written in the form:

$$\begin{aligned} I_h(m, \dots, m) &= \left(\frac{m}{2\pi^2} \right)^4 \int d^3p \int d^3q \frac{1}{p^2 + m^2} \frac{1}{q^2 + m^2} g(|p|, |q|, \theta)^2 \\ &= \frac{1}{2\pi^6} \int_0^\infty dx \int_0^\infty dy \int_0^\pi d\theta \sin \theta \frac{x^2}{x^2 + 1} \frac{y^2}{y^2 + 1} g(x, y, \theta, m=1)^2. \end{aligned} \quad (6.6)$$

The function g can be obtained most easily by introducing two Feynman parameters before evaluating the momentum integral:

$$\begin{aligned}
& g(x, y, \theta, m = 1) \\
&= \int d^3s \int_0^1 dw \int_0^1 dz \frac{2z}{(s^2 + 1 + wz x^2 + (1-z)y^2 - 2s \cdot (wz \bar{x} + (1-z)\bar{y}))^3} \\
&= \frac{\pi^2}{2} \int_0^1 dw \int_0^1 dz \frac{z}{(1 + wz(1-wz) x^2 + z(1-z) y^2 - 2wz(1-z) xy \cos \theta)^{3/2}} \\
&= \pi^2 \int_0^1 dw \frac{2 + y^2 + w x^2 - 2\sqrt{1+w(1-w)} x^2 - 2w xy \cos \theta}{\sqrt{1+w(1-w)} x^2} \\
&\times \left(w^2 x^2 (4 - 4xy \cos \theta + x^2) + y^2 (4 - 4wxy \cos \theta + y^2) \right. \\
&\left. + 2wx^2 y^2 (1 + 2w(\cos \theta)^2) - 8wxy \cos \theta \right)^{-1}. \tag{6.7}
\end{aligned}$$

The remaining w -integral can, too, be calculated and yields merely elementary functions, but the result is far too long to be printed here. Using (6.7) one may now anyway perform the numerical integral of (6.6), which eventually leads to the result for the wheel diagram

$$I_h(m, \dots, m) \approx 0.005. \tag{6.8}$$

Diagram i

The numerical evaluation of the H diagram is very similar to the preceding case. Setting all masses the same one is able to write the integral in the form

$$\begin{aligned}
I_i(m, \dots, m) &= \left(\frac{m}{2\pi^2} \right)^4 \int d^3p \int d^3q \frac{1}{p^2 + m^2} \frac{1}{q^2 + m^2} \frac{1}{(q-p)^2 + m^2} g(|p|, |q|, \theta)^2 \tag{6.9} \\
&= \frac{1}{2\pi^6 m^2} \int_0^\infty dx \int_0^\infty dy \int_0^\pi d\theta \sin \theta \frac{x^2}{x^2 + 1} \frac{y^2}{y^2 + 1} \frac{g(x, y, \theta, m = 1)^2}{x^2 + y^2 - 2xy \cos \theta + 1}.
\end{aligned}$$

The final numerical integration is easily performed using the expression for g given in (6.7) and yields

$$I_i(m, \dots, m) \approx 0.0009 \times m^{-2}. \tag{6.10}$$

Diagram j

The 'twisted H' diagram is especially difficult to evaluate, and one is even unable to take advantage of the known form of the g -function constructed above. The most straightforward way to proceed is to first combine the different propagators by introducing multiple Feynman parameters and then to use standard formulae to perform the momentum integrals. In the

end one is, however, left with several one-dimensional integrals that have to be evaluated numerically.

Using the standard parametrization formula (see e.g. [37])

$$\frac{1}{(D_1)^{a_1} \dots (D_k)^{a_k}} = \frac{\Gamma(a_1 + a_2 + \dots + a_k)}{\Gamma(a_1) \Gamma(a_2) \dots \Gamma(a_k)} \int_0^1 \prod_{i=1}^k dx_i \frac{\delta(1 - x_1 - \dots - x_k) x_1^{a_1-1} \dots x_k^{a_k-1}}{(D_1 x_1 + \dots + D_k x_k)^{a_1 + \dots + a_k}} \quad (6.11)$$

one obtains:

$$\begin{aligned} I_j(m, \dots, m) &\equiv \int_{p,q,r,s} \frac{1}{p^2 + m^2} \frac{1}{q^2 + m^2} \frac{1}{r^2 + m^2} \frac{1}{s^2 + m^2} \frac{1}{(p-r)^2 + m^2} \\ &\times \frac{1}{(p-s)^2 + m^2} \frac{1}{(q-r)^2 + m^2} \frac{1}{(q-s)^2 + m^2} \frac{1}{(p+q-r-s)^2 + m^2} \\ &= \Gamma(9) \int_{p,q,r,s} \int_0^1 \prod_{i=1}^9 dx_i \delta\left(1 - \sum_{i=1}^9 x_i\right) \left(m^2 + p^2 \overbrace{(x_1 + x_5 + x_6 + x_9)}^{y_1}\right. \\ &\quad \left.+ q^2 \overbrace{(x_2 + x_7 + x_8 + x_9)}^{y_2} + r^2 \overbrace{(x_3 + x_5 + x_7 + x_9)}^{y_3} + s^2 \overbrace{(x_4 + x_6 + x_8 + x_9)}^{y_4}\right. \\ &\quad \left.- 2p \cdot r (x_5 + x_9) - 2p \cdot s (x_6 + x_9) - 2q \cdot r (x_7 + x_9)\right. \\ &\quad \left.- 2q \cdot s (x_8 + x_9) + 2p \cdot q x_9 + 2r \cdot s x_9\right)^{-9}. \end{aligned} \quad (6.12)$$

The momentum integrations can now be performed using the simple relation

$$\int d^{2\omega} p \frac{1}{(p^2 + m^2 + 2p \cdot q)^m} = \frac{\pi^\omega \Gamma(m - \omega)}{\Gamma(m)} \frac{1}{(m^2 - q^2)^{m-\omega}}, \quad (6.13)$$

which leads to:

$$I_j(m, \dots, m) = \frac{1}{8\pi^2 m^2} \int_0^1 \prod_{i=1}^9 dx_i \frac{\delta\left(1 - \sum_{i=1}^9 x_i\right) y_1^{9/2} A^{3/2}}{\left((AC - E^2)(AB - D^2) - (AF - DE)^2\right)^{3/2}}. \quad (6.14)$$

The functions A, ..., F in the final form are

$$\begin{aligned} A &= y_1 y_2 - x_9^2 \\ B &= y_1 y_3 - (x_5 + x_9)^2 \\ C &= y_1 y_4 - (x_6 + x_9)^2 \\ D &= y_1 (x_7 + x_9) - x_9 (x_5 + x_9) \\ E &= y_1 (x_8 + x_9) - x_9 (x_6 + x_9) \\ F &= y_1 x_9 - (x_5 + x_9)(x_6 + x_9). \end{aligned}$$

Evaluating the parametric integrals numerically one finally gets

$$I_j(m, \dots, m) \approx 0.0004 \times m^{-2}. \quad (6.15)$$

6.2 Partial differential equations

As another method of tackling the evaluation of the integrals of this chapter let us now derive partial differential equations with respect to the propagator masses that the diagrams f to i must satisfy. This will be done in analogy with the treatment of the Mercedes diagram in [20] and will employ the idea developed by Kotikov [39]. However, as already mentioned, finding solutions to the equations obtained here seems to be a laborious task - probably one requiring the use of numerical methods - and that question will not be addressed in the thesis.

In the following let us use a compact notation for the propagators and diagrams adopted from [20]. A propagator with momentum p and mass m_a will be denoted by Δ_p^a , a diagram I with one propagator (mass m_a) squared by K_a and the same diagram with one propagator (mass m_a) squared and one propagator (mass m_b) removed by J_a^b .

Consider then a convergent ($\epsilon = 0$) planar four-loop diagram with the structure

$$I \equiv \int_{p,q,r,s} \Delta_p^1 \Delta_{p-q}^2 \Delta_{p-r}^3 \Delta_q^4 \Delta_r^5 f(q, r, s), \quad (6.16)$$

where f is an in principle arbitrary function of three variables. This is illustrated by the figure below and appears in all integrals considered here.

$$\begin{array}{c} \diagup 2 \quad \diagdown 3 \\ \diagdown 4 \quad \diagup 5 \\ \text{---} 1 \text{---} \end{array} \quad (6.17)$$

Performing a partial integration with respect to p and neglecting the vanishing boundary terms one obtains:

$$\begin{aligned} I &= -\frac{1}{3} \int_{p,q,r,s} p_i \frac{\partial}{\partial p_i} \left[\Delta_p^1 \Delta_{p-q}^2 \Delta_{p-r}^3 \Delta_q^4 \Delta_r^5 f(q, r, s) \right] \\ &= \frac{2}{3} \int_{p,q,r,s} \Delta_p^1 \Delta_{p-q}^2 \Delta_{p-r}^3 \Delta_q^4 \Delta_r^5 f(q, r, s) \left(p^2 \Delta_p^1 + p \cdot (p-q) \Delta_{p-q}^2 + p \cdot (p-r) \Delta_{p-r}^3 \right) \\ &= \frac{2}{3} \int_{p,q,r,s} \Delta_p^1 \Delta_{p-q}^2 \Delta_{p-r}^3 \Delta_q^4 \Delta_r^5 f(q, r, s) \\ &\quad \times \left(1 - m_1^2 \Delta_p^1 - m_1^2 \Delta_{p-q}^2 + \left(\Delta_p^1 \right)^{-1} \Delta_{p-q}^2 - m_1^2 \Delta_{p-r}^3 + \left(\Delta_p^1 \right)^{-1} \Delta_{p-r}^3 \right. \\ &\quad \left. + \frac{1}{2} \left[1 + \left(-m_2^2 - \left(\Delta_p^1 \right)^{-1} + m_1^2 - \left(\Delta_q^4 \right)^{-1} + m_4^2 \right) \Delta_{p-q}^2 \right] \right. \\ &\quad \left. + \frac{1}{2} \left[1 + \left(-m_3^2 - \left(\Delta_p^1 \right)^{-1} + m_1^2 - \left(\Delta_r^5 \right)^{-1} + m_5^2 \right) \Delta_{p-r}^3 \right] \right) \end{aligned} \quad (6.18)$$

$$\Leftrightarrow I = 2m_1^2 K_1 + \left(m_1^2 + m_2^2 - m_4^2 \right) K_2 + \left(m_1^2 + m_3^2 - m_5^2 \right) K_3 - J_2^1 - J_3^1 + J_2^4 + J_3^5, \quad (6.19)$$

which is equivalent to eq. 29 of [20] (up to a few misprints in [20]).

Using the above result one is able to write down partial differential equations for all diagrams of this chapter with the exception of the non-planar 'twisted H' -case. The equations are of first order and can in principle be solved by standard methods starting from the g and

f cases. For these two diagrams the equations contain as parameters values of only such diagrams that have already been evaluated in this thesis with arbitrary masses. Below I shall merely list the equations.

Diagram f

$$\begin{aligned}
& \left(1 + 2m_1^2 \frac{\partial}{\partial m_1^2} + (m_1^2 + m_2^2 - m_4^2) \frac{\partial}{\partial m_2^2} + (m_1^2 + m_3^2 - m_5^2) \frac{\partial}{\partial m_3^2} \right) I_f \quad (6.20) \\
&= \frac{\partial}{\partial m_2^2} I_b(m_2, m_3, m_4, m_5, m_7, m_8, m_6) + \frac{\partial}{\partial m_3^2} I_b(m_2, m_3, m_4, m_5, m_7, m_8, m_6) \\
&\quad - \frac{\partial}{\partial m_2^2} I_c(m_1, m_5, m_7, m_8, m_3, m_6, m_2) - \frac{\partial}{\partial m_3^2} I_c(m_1, m_4, m_7, m_8, m_2, m_6, m_3)
\end{aligned}$$

Diagram g

$$\begin{aligned}
& \left(1 + 2m_1^2 \frac{\partial}{\partial m_1^2} + (m_1^2 + m_2^2 - m_4^2) \frac{\partial}{\partial m_2^2} + (m_1^2 + m_3^2 - m_5^2) \frac{\partial}{\partial m_3^2} \right) I_g \quad (6.21) \\
&= \frac{\partial}{\partial m_2^2} I_a(m_2, m_3, m_4, m_5, m_6, m_7) + \frac{\partial}{\partial m_3^2} I_a(m_2, m_3, m_4, m_5, m_6, m_7) \\
&\quad - \frac{\partial}{\partial m_2^2} I_e(m_3, m_1, m_5, m_8, m_2, m_6, m_7) - \frac{\partial}{\partial m_3^2} I_e(m_2, m_1, m_4, m_8, m_3, m_6, m_7)
\end{aligned}$$

Diagram h

$$\begin{aligned}
& \left(1 + 2m_1^2 \frac{\partial}{\partial m_1^2} + (m_1^2 + m_2^2 - m_4^2) \frac{\partial}{\partial m_2^2} + (m_1^2 + m_3^2 - m_5^2) \frac{\partial}{\partial m_3^2} \right) I_h \quad (6.22) \\
&= \frac{\partial}{\partial m_2^2} I_g(m_8, m_4, m_5, m_6, m_7, m_2, m_3) + \frac{\partial}{\partial m_3^2} I_g(m_8, m_4, m_5, m_6, m_7, m_2, m_3) \\
&\quad - \frac{\partial}{\partial m_2^2} I_g(m_5, m_1, m_8, m_3, m_7, m_2, m_6) - \frac{\partial}{\partial m_3^2} I_g(m_4, m_1, m_8, m_2, m_6, m_3, m_7)
\end{aligned}$$

Diagram i

$$\begin{aligned}
& \left(1 + 2m_1^2 \frac{\partial}{\partial m_1^2} + (m_1^2 + m_2^2 - m_4^2) \frac{\partial}{\partial m_2^2} + (m_1^2 + m_3^2 - m_5^2) \frac{\partial}{\partial m_3^2} \right) I_i \quad (6.23) \\
&= \frac{\partial}{\partial m_2^2} I_h(m_6, m_2, m_4, m_7, m_9, m_3, m_5, m_8) + \frac{\partial}{\partial m_3^2} I_h(m_6, m_2, m_4, m_7, m_9, m_3, m_5, m_8) \\
&\quad - \frac{\partial}{\partial m_2^2} I_f(m_5, m_1, m_9, m_3, m_8, m_7, m_2, m_6) - \frac{\partial}{\partial m_3^2} I_f(m_4, m_1, m_9, m_2, m_6, m_7, m_3, m_8)
\end{aligned}$$

Chapter 7

Conclusions

Based on the complexity of already existing three-loop computations ([19, 20], etc.) and the fact that even at this order one has been forced to resort to numerical methods, the evaluation of four-loop scalar diagrams could already in advance be anticipated to be a highly non-trivial task. The two-particle irreducible diagrams, skeletons, represent furthermore an especially tedious subset of these, since no immediate way is available for reducing the integrals into lower-order calculations. In this thesis it has been observed that these fears are indeed well-motivated. One has, however, also seen that even analytic results can be obtained for diagrams which at first sight appear to be extremely complicated.

Of the ten diagrams considered here I have been able to evaluate completely analytically two while keeping the masses of the propagators arbitrary. For three other ones simple one- or two-dimensional integral representations have been constructed with arbitrary masses, and when setting the masses equal one of these integrals has been shown to be analytically calculable. With the exception of one special case the evaluation of the remaining diagrams with equal propagator masses has too been reduced to the calculation of two- and three-dimensional integrals that can easily be performed numerically. In the identical mass -case explicit numerical results have been given for all diagrams of this thesis making a direct comparison of their magnitudes possible. It is in addition notable that all divergent parts of the diagrams have been determined analytically.

The fact that I have failed to obtain simple results for the finite parts of some integrals certainly does not imply that this task would be insurmountable. Analytic expressions for the diagrams surely exist and to obtain them one merely needs to do more work: there are a great number of different calculational techniques and tricks left to try. A lot of effort is also required in evaluating all the additional diagrams that perturbative calculations in three-dimensional effective QCD will produce.

It is evident that much remains to be done in the field of evaluating multi-loop Feynman diagrams. A need for such calculations is present in many areas of modern day physics and new techniques for the analytic treatment of diagrams are constantly emerging (see e.g. [17, 41, 40]). Research in the field will certainly remain active for years to come.

Bibliography

- [1] H. Fritzsche, M. Gell-Mann and H. Leutwyler, Phys. Lett. B 47 (1973) 365;
H.D. Politzer, Phys. Rev. Lett. 26 (1973) 1346;
D.J. Gross and F. Wilczek, Phys. Rev. Lett. 26 (1973) 1343.
- [2] J.C. Collins and M.J. Perry, Phys. Rev. Lett. 34 (1975) 1353.
- [3] F. Karsch, E. Laermann and A. Peikert, Nucl. Phys. B 605 (2001) 579.
- [4] D.J. Gross, R. Pisarski and L. Yaffe, Rev. Mod. Phys. 53 (1981) 43.
- [5] J. Kapusta, "Finite temperature field theory", Cambridge (1989).
- [6] A. Peshier, (1999) [hep-ph/9910451].
- [7] F. Karsch, (2001) [hep-lat/0106019].
- [8] S. Hands, (2001) [hep-lat/0109034].
- [9] G. Boyd et al., Nucl. Phys. B 469 (1996) 419 [hep-lat/9602007].
- [10] M. Okamoto et al., Phys. Rev. D 60 (1999) 094510 [hep-lat/9905005].
- [11] A.D. Linde, Phys. Lett. B 96 (1980) 289.
- [12] E. Braaten, Phys. Rev. Lett. 74 (1995) 2164-2167 [hep-ph/9409434].
- [13] E. Braaten and A. Nieto, Phys. Rev. D 51 (1995) 6990-7006 [hep-ph/9501375].
- [14] K. Kajantie, M. Laine, K. Rummukainen and Y. Schröder, Phys. Rev. Lett. 86 (2001) 10-13 [hep-ph/0007109].
- [15] K. Kajantie, M. Laine and Y. Schröder, (2001) [hep-ph/0109100].
- [16] J.A.M. Vermaseren, [math-ph/0010025]; <http://www.nikhef.nl/~form/>.
- [17] D.J. Broadhurst, Z. Phys. C 54 (1992) 599.
- [18] L.V. Avdeev, Comput. Phys. Commun. 98 (1996) 15-19 [hep-ph/9512442].

- [19] S. Groote, J.G. Körner and A.A. Pivovarov, Phys. Lett. B 443 (1998) 269 [hep-ph/9805224].
- [20] A.K. Rajantie, Nucl. Phys. B 480 (1996) 729-752; Erratum-ibid. B513 (1998) 761-762 [hep-ph/9606216].
- [21] E. Braaten and A. Nieto, Phys. Rev. D 53 (1996) 3421 [hep-ph/9510408].
- [22] K. Kajantie, M. Laine, K. Rummukainen and M. Shaposhnikov, Nucl. Phys. B 503 (1997) 357 [hep-ph/9704416];
K. Kajantie, M. Laine, J. Peisa, A. Rajantie, K. Rummukainen and M. Shaposhnikov, Phys. Rev. Lett. 79 (1997) 3130 [hep-ph/9707207].
- [23] A. Hart, M. Laine and O. Philipsen, Nucl. Phys. B 586 (2000) 443 [hep-ph/0004060].
- [24] K. Farakos, K. Kajantie, K. Rummukainen, M. Shaposhnikov Nucl. Phys. B 425 (1994) 67 [hep-ph/9404201].
- [25] D. Bailin and A. Love, Introduction to gauge field theory, IOP (1993).
- [26] E. Shuryak, J. E. T. P. 47 (1978) 212.
- [27] J. Kapusta, Nucl. Phys. B 148 (1979) 461.
- [28] T. Toimela, Phys. Lett. B 124 (1983) 407.
- [29] P. Arnold and C. Zhai, Phys. Rev. D 50 (1994) 7603 [hep-ph/9408276]; *ibid.* 51 (1995) 1906 [hep-ph/9410360].
- [30] C. Zhai and B. Kastening, Phys. Rev. D 52 (1995) 7232 [hep-ph/9507380].
- [31] T. Appelquist and J. Carazzone, Phys. Rev. D 11 (1975) 2856.
- [32] C. Korthals Altes, Nucl. Phys. B 420 (1994) 637.
- [33] J.-P. Blaizot, E. Iancu and A. Rebhan, Phys. Rev. Lett. 83 (1999) 2906 [hep-ph/9906340]; Phys. Rev. D63 (2001) 065003 [hep-ph/0005003]; 2001 [hep-ph/0104033].
- [34] J.M. Luttinger and J.C. Ward, Phys. Rev. 118 (1960) 1417;
G. Baym, Phys. Rev. 127 (1962) 1391;
C. De Dominicis and P.C. Martin, J. Math. Phys. 5 (1964) 31.
- [35] J.M. Cornwall, R. Jackiw and E. Tomboulis, Phys. Rev. D 10 (1974) 2428.
- [36] B. Kastening, Phys. Rev. D 54 (1996) 3965 [hep-ph/9604311].
- [37] P. Ramond, "Field Theory - a Modern Primer", Benjamin/Cummings (1981).
- [38] I.S. Gradshteyn and I.M. Ryzhik, "Table of Integrals, Series and Products", 6th edition, Academic Press (2000).

- [39] A.V. Kotikov, Phys. Lett. B 254 (1991) 158; Mod. Phys. Lett. A 6 (1991) 677.
- [40] B. Kastening, Phys. Lett. A 269 (2000) 50 [hep-ph/9909017].
- [41] G. Passarino, (2001) [hep-ph/0108252].
- [42] E. Braaten and A. Nieto, Phys. Rev. Lett. 76 (1996) 1417 [hep-ph/9508406].
- [43] B. Peterson, (2000) [hep-lat/0009016].